การเปลี่ยนสถานะทางโครงสร้างของโลหะลิเธียมของแข็งโดยวิธีคลื่นระนาบที่แต่งเติม

นายอภิรัตน์ ภูษิตตระกูล

วิทยานิพนธ์นี้เป็นส่วนหนึ่งของการศึกษาตามหลักสูตรปริญญาวิทยาศาสตรมหาบัณฑิต
สาขาวิชาฟิสิกส์ ภาควิชาฟิสิกส์
คณะวิทยาศาสตร์ จุฬาลงกรณ์มหาวิทยาลัย
ปีการศึกษา 2546

ISBN 974-17-4779-9

STRUCTURAL PHASE TRANSITIONS IN SOLID LITHIUM METAL BY AUGMENTED PLANE WAVE METHOD

Mr. Apirath Phusittrakool

A Thesis Submitted in Partial Fulfillment of the Requirements
for the Degree of Master of Science in Physics
Department of Physics
Faculty of Science
Chulalongkorn University
Academic year 2003
ISBN 974-17-4779-9

Thesis Title	Structural phase transitions in solid lithium metal by augmented plane wave method
By	Mr. Apirath Phusittrakool
Field of Study	Physics
Thesis Advisor	Assistant Professor Udomsilp Pinsook, Ph.D.

Accepted by the Faculty of Science, Chulalongkorn University in Partial Fulfillment of the Requirements for the Master's Degree

..... Dean of the Faculty of Science
(Professor Piamsak Menasveta, Ph.D.)

THESIS COMMITTEE

..... Chairman
(Associate Professor Wichit Sritrakool, Ph.D.)

..... Thesis Advisor
(Assistant Professor Udomsilp Pinsook, Ph.D.)

..... Member
(Assistant Professor Kajornyod Yoodee, Ph.D.)

..... Member
(Somchai Kiatgamolchai, Ph.D.)

อภิรัตน์ ภูษิตตระกูล : การเปลี่ยนสถานะทางโครงสร้างของโลหะลิเธียมของแข็งโดยวิธีคลื่นระนาบที่แต่งเติม. (STRUCTURAL PHASE TRANSITIONS IN SOLID LITHIUM METAL BY AUGMENTED PLANE WAVE METHOD) อ. ที่ปรึกษา : ผู้ช่วยศาสตราจารย์ ดร. อุดม ศิลป์ ปิ่นสุข, จำนวนหน้า 58 หน้า. ISBN 974-17-4779-9.

กระบวนการในการคำนวณหาพลังงานรวมของของแข็งที่มีความถูกต้องสูงได้ถูกพัฒนาขึ้นและถูกนำไปใช้ในการหาคุณสมบัติทางโครงสร้างของลิเธียม (lithium) การคำนวณจะอาศัยทฤษฎีฟังก์ชันนัลความหนาแน่นแบบเฉพาะที่ (local-density-functional) และวิธีการคลื่นระนาบที่แต่งเติมเชิงเส้นแบบศักย์เต็มรูป (full-potential linearized augmented-plane-wave) เราได้ใช้กระบวนการนี้คำนวณหากราฟความสัมพันธ์ของพลังงานรวมกับปริมาตรสำหรับโครงสร้างผลึก sc, bcc, fcc และ hcp ของลิเธียม เพื่อที่จะนำมาใช้ในการศึกษาสมบัติทางโครงสร้างต่างๆ อาทิเช่น ค่าคงตัวแลททิซ (lattice constant), โมดูลัสเชิงปริมาตร (bulk modulus) เป็นต้น ค่าของพลังงานรวมที่คำนวณได้นั้นมีความเที่ยงตรงมากกว่า 0.5 มิลลิริดเบอร์ก (mRy) ผลของสมบัติทางโครงสร้างที่ได้สอดคล้องกับผลของคนอื่นและผลจากการทดลอง นอกจากนี้แล้วเรายังได้ใช้กระบวนการนี้เพื่อศึกษาโครงสร้างแถบพลังงาน (band structure) และความหนาแน่นของอิเล็กตรอน (electron density) ของลิเธียมภายใต้สภาวะความดันอีกด้วย

ภาควิชา ฟิสิกส์ ลายมือชื่อนิสิต .....
สาขาวิชา ฟิสิกส์ ลายมือชื่ออาจารย์ที่ปรึกษา .....
ปีการศึกษา 2546

4372479223 :MAJOR PHYSICS
KEY WORDS: TOTAL ENERGY / DFT / FLAPW / ELECTRONIC STRUCTURE / STRUCTURAL PROPERTIES / BULK LITHIUM

APIRATH PHUSITTRAKOOL : STRUCTURAL PHASE TRANSITIONS IN SOLID LITHIUM METAL BY AUGMENTED PLANE WAVE METHOD. THESIS ADVISOR : ASST. PROF. UDOMSILP PINSOOK, PH.D., 58 pp. ISBN 974-17-4779-9.

A procedure for calculating the highly accurate total energy of bulk solids has been developed and applied to determine the structural properties of lithium. The formalism is based on the local-density-functional theory and the full-potential linearized augmented-plane-wave method. This procedure was used to obtain the total-energy curves for the sc, bcc, fcc and hcp phases of Li from which a number of structural properties (lattice constant, bulk modulus, etc.) were derived. The calculated total energies have a precision better than 0.5 mRy. The resulting structural properties are in agreement with other calculations and experiments. The band structure and the electron density of Li under pressure are also presented and compared to the zero-pressure results.

Department Physics — Student's signature .....

Field of study Physics — Advisor's signature .....

Academic year 2003

Acknowledgements

I deeply appreciate the valuable contributions of a number of people and would like to acknowledge them. I am particularly grateful to my advisor, Asst. Prof. Udomsilp Pinsook, for introducing and inspiring me to the field of computational condensed matter physics, and giving me an opportunity to work in his research group. I greatly appreciate his guidance throughout the work. I would like to thank Dr. Thiti Borvornratanaraks for providing the results from the program package CASTEP. I also thank Mr. Pairot Moontragoon for useful discussions in developing the program.

I wish to thank Assoc.Prof. Wichit Sritrakool, Asst.Prof. Kajornyod Yoodee and Dr. Somchai Kiatgamolchai for taking the time from their busy schedules to be on my thesis committee. Their comments on this thesis are also greatly appreciated.

Lastly, I would like to thank many good friends of mine, especially, Miss Suwakan Piankoranee, who is always beside me. Their supports, cheer and encouragement made me strong to get through this hard work.

Table of Contents

List of Figures

List of Symbols

α	muffin-tin sphere index
$\varepsilon_{\nu\mathbf{k}}$	energy eigenvalue
ε_{xc}	exchange-correlation energy per electron
$\phi_{\mathbf{G}}$	basis function expansion of wave function
ν	band index
$\rho(\mathbf{r})$	charge density
$\Theta(\mathbf{r} \in \mathcal{R})$	unit step function, whose value is one for $\mathbf{r}$ in the region $\mathcal{R}$ and zero elsewhere
$\Theta_{\mathbf{G}}$	Fourier transform of step function $\Theta(\mathbf{r} \in \mathrm{I})$
Ψ	many-body wave function
ψ_i, $\psi_\nu(\mathbf{k})$	single-particle wave function
Ω	unit-cell volume
A_L, B_L	coefficient of spherical harmonic expansion of the basis function
$c_{\mathbf{G}}$	expansion coefficient of wave function
e	electron charge
E_ℓ	linearization energy parameter
E_{tot}	total energy
$\hat{H}$	Hamiltonian operator
$H_{\mathbf{G}\mathbf{G}'}$	Hamiltonian matrix element
$\mathbf{G}$	reciprocal lattice vector
$\|\mathbf{G}\|, G$	magnitude of vector $\mathbf{G}$
$\mathbf{k}$	wave vector
$\hat{\mathbf{k}}$	angular coordinates of vector $\mathbf{k}$
$\mathbf{k}_{\mathbf{G}}$	$\equiv \mathbf{k} + \mathbf{G}$
L	abbreviation of the angular quantum number (ℓ, m)
$n(\mathbf{r})$	electron density
$n_{\mathbf{G}}$	coefficient of Fourier expansion of $n(\mathbf{r})$

$\mathbf{r}$	position vector; $\mathbf{r} = \mathbf{r}_\alpha + \mathbf{r}'$ (see Figure 2.2b)
$\hat{\mathbf{r}}$	represent the angular coordinates (θ, ϕ) of vector $\mathbf{r}$
$\mathbf{r}'$	local coordinates, origin at center of the sphere
$\mathbf{r}_\alpha$	position of the αth muffin-tin sphere
R_α	muffin-tin sphere radius
$\mathbf{R}_I$, $\mathbf{R}_J$	position of nucleus
$S_{\mathbf{GG}'}$	overlap matrix element
u_ℓ	solution of radial Schrödinger equation
$\dot{u}_\ell$	$\equiv \frac{\partial u_\ell}{\partial E}$
u'_ℓ	$\equiv \frac{\partial u_\ell}{\partial r'}$
$V(\mathbf{r})$	potential energy function
V_{eff}	effective potential
V_C	Coulomb potential
V_{xc}	exchange-correlation potential
$w_{\nu j}$	weight for integrating over Brillouin zone
$Y_L(\hat{\mathbf{r}})$	spherical harmonic function
Z_I	atomic number of the atom at position $\mathbf{R}_I$

APW+lo	Augmented Plane Wave plus local orbitals
BZ	Brillouin Zone
DFT	Density Functional Theory
FLAPW	Full-potential Linearized Augmented-Plane-Wave
FFT	Fast Fourier Transform
KS	Kohn-Sham
LDA	Local Density Approximation
I	Interstitial region
MT	Muffin-Tin sphere region

Chapter 1

Introduction

Simulating real materials has become increasingly more important in understanding a variety of modern topics in condensed matter and surface physics as well as quantum chemistry. The increasing number of new highly sophisticated experimental techniques, coupled with the development of an increasing variety of new materials with new properties has driven the need for a more accurate theoretical understanding at the atomic scale. This has led to the increasing use of *ab initio*[1] (first-principle) study where the quantum mechanical behavior of electrons is explicitly treated. The advantage of *ab initio* methods lies in the fact that they can be carried out without knowing any experimental data of the system. Nowadays, the advance in theoretical-computational techniques for a tractable quantum mechanical treatment combined with the growing power of computers allows the accurate simulation of materials and understanding of their behavior at the atomic-scale. Also, using the computational approach enables the design of new materials and the prediction of the properties which would be impossible or impractical to obtain experimentally.

An important breakthrough in the *ab initio* calculations was the development of density functional theory (DFT), which states that under certain conditions all ground-state properties of matter are completely determined by the charge density of the electrons. In principle, density functional theory permits the accurate evaluation of the electronic part of the total energy and, consequently, after including the Coulomb interaction between the nuclei it enables the evaluation of all structural properties.

[1] Ab initio is a Latin phrase that means "from the beginning". It is usually referred to the calculation of properties by solving Schrödinger equations directly.

Nearly all physical properties are related to the total energies or to differences between the total energies. If the total energies can be calculated, any physical property related to the total energy can be determined computationally. For instance, the equilibrium lattice constant of a crystal is the lattice constant that minimizes the total energy. To predict the equilibrium lattice constant of a crystal, a series of total-energy calculations are performed to determine the total energy as a function of the lattice constant, and a smooth curve is constructed through them. The theoretical value for the equilibrium lattice constant is determined at the minimum of the curve. Another property derived from the total-energy calculations is the crystal stability. We can predict a preferred ground-state structure by comparing the total energies between different structures. Total-energy techniques have also been successfully used to predict bulk moduli, cohesive energies, and phase-transitions due to pressure and temperature (for reviews see [1]).

The differences in energy among the crystal structures are often rather small; thus high accuracy in the total-energy calculations is required. A successful approach is the implementation of the full-potential linearized augmented-plane-wave (FLAPW) method [2, 3, 4], which allows one to treat the total energy to high accuracy without resorting to frozen-core, pseudopotential, or other approximations. The FLAPW method is considered as the most accurate all-electron method for computation of electronic structures based on density functional theory. There are several programs employing this method such as the WIEN code [5], FLAPW (Freeman's group), FLEUR (Blügel's group), D. Singh's code and others.

In this work, we aim to develop and implement an all-electron total-energy calculation for microscopic study of electronic and structural properties of bulk solids. The method is based on the local-density-functional theory with the FLAPW approach. Although our formalism for evaluating the total energy is similar in many respects to those [2, 4, 6, 7, 8, 9, 10], we have constructed our own algorithm. As a correctness test of our method, we have applied it to the bulk lithium (Li).

Lithium, a monovalent metal ($1s^2 2s^1$), is considered as a simple metal. Under ordinary conditions of pressure and temperature, the motion of conduction electrons is only weakly perturbed by interactions with the atomic cores. Although its electronic structure is relatively simple, its structural properties still pose a

significant challenge to both experiment and simulation. Li is known to undergo a structural phase transformation from the bcc to 9R (a nine-layer hexagonal close-packed structure, stacking ABCBCACAB) and fcc phases when cooled down to 77 K at ambient pressure [11]. Moreover, it transforms to several phases when compressed [12, 13]. Because Li is very soft, the determination of its structural properties requires very delicate experiment as well as simulation of high numerical accuracy. The studies of Li are of fundamental interest, because they are expected to be a theoretical model of hydrogen, and also may reveal new aspects and new properties.

This thesis is organized as follows. In Chapter 2, we discuss an overview of theoretical background for the method used in calculating the total energy of bulk solids. The basics of density functional theory and the concepts of the FLAPW method are briefly reviewed, and the procedures for the total-energy calculations are explained. In Chapter 3, some of the details and practical aspects of our implementation of the method are described. Chapter 4 contains the results of our calculation of the total energies for bulk lithium. The results including static structural properties, crystal stability and electronic structure are discussed and compared with previous calculations and experiment. Finally, we summarize our conclusions in Chapter 5. A flow chart of our algorithm is presented in Appendix A, and the detail of Numerov's method is given in Appendix B.

Chapter 2

Theoretical Discussion

A solid consists of a collection of atomic nuclei and electrons. These particles interact with each other by the electromagnetic force. This is a quantum many-body problem. It is possible, at least in principle, to determine theoretically all the properties of a solid by solving the quantum-mechanical problem for that solid state system. However, solving a many-body problem is a formidable task. Approximations are required to simplify the problem. Because the nuclei are much heavier and therefore much slower than the electrons, we can assume that the electrons respond essentially instantaneously to the motions of the nuclei. Thus the nuclei can be treated as they are still at fixed positions. This is known as the *Born-Oppenheimer approximation*. After having applied this approximation, the problem reduces to the dynamics of the electrons in some frozen configurations of the nuclei. The Schrödinger equation of the system becomes

$$\hat{H}\Psi(\mathbf{r}_1, \mathbf{r}_2, \ldots, \mathbf{r}_N) = E\Psi(\mathbf{r}_1, \mathbf{r}_2, \ldots, \mathbf{r}_N), \tag{2.1}$$

and the Hamiltonian is given by

$$\hat{H} \equiv \sum_i \left[-\frac{\hbar^2}{2m}\nabla_i^2 - \frac{1}{4\pi\epsilon_0}\sum_I \frac{e^2 Z_I}{|\mathbf{r}_i - \mathbf{R}_I|} + \frac{1}{8\pi\epsilon_0}\sum_{j\neq i}\frac{e^2}{|\mathbf{r}_i - \mathbf{r}_j|} \right],$$

where the first term in the square bracket is the kinetic energy operator of the electrons, the second is the electron-nucleus interaction and the third term is the interaction among the electrons.

Even with this simplification, however, solving for a many-electron wave function Ψ is still extremely difficult. Several methods exist to reduce Eq. (2.1) to an approximate but feasible form. A historically very important one is the Hartree-Fock method (HF), but it can be applied only to tiny systems. In order to

deal with solids, another approach commonly used to describe complex electronic systems is *density functional theory* (DFT).

2.1 Density Functional Theory

Density functional theory (DFT) is one of the most popular and successful quantum mechanical approaches to matter. It is nowadays broadly applied to calculate electronic properties of materials and molecules such as binding energy and band structures. The success of DFT comes from two important theories which were developed by Hohenberg-Kohn [14] and Kohn-Sham [15] in the mid-1960s. The underlying idea is to focus on the density of the electrons rather than the many-body wave functions, and hence all ground-state properties can be derived from the electron density.

2.1.1 Hohenberg-Kohn theorems

Hohenberg and Kohn were able to show, for systems with a non-degenerate ground-state, that:

- There exists a *one-to-one* mapping between the ground-state density $n(\mathbf{r})$ of a many-electron system and the external potential V_{ext}. Consequently, the ground-state energy E and all other ground-state properties of the system are unique functionals of the electron density, i.e.

$$E \equiv E[n(\mathbf{r})]. \tag{2.2}$$

- For a given external potential, the *correct* ground-state density n_0 minimize the energy functional $E[n]$, and only the minimum value of $E[n]$ is equal to the ground-state total energy of the system:

$$E_{tot} = E[n_0] \leq E[n]. \tag{2.3}$$

The second part of theorem makes it possible to use the variational principle in order to find the ground-state density. However, no explicit representation of $E[n]$ has been derived so far. But having found n_0, all knowledge about the system is found.

2.1.2 Kohn-Sham equations

The equations of Kohn and Sham have turned DFT into a practical tool for the numerical determination of the ground-state density. In the Kohn-Sham formulation, the Hohenberg-Kohn energy functional $E[n]$ is split into the following terms:

$$E[n] = T_s[n] + U[n] + E_{xc}[n], \tag{2.4}$$

where T_s is the kinetic energy of *non-interacting* electrons, U is the potential energy which consists of the coulomb energy of the interaction of the electrons and the interaction with an external potential (for a solid it is usually a coulomb potential due to the nuclei), and the last term, E_{xc}, contains the exchange and correlation effects as well as a correction to the kinetic energy due to the interaction of the electrons.

With the introduction of the functional $T_s[n]$, then applying the variational principle to the Eq. (2.4), this leads to a set of equations known as the Kohn-Sham (KS) equations:

$$\hat{H}_{\text{KS}}\psi_i(\mathbf{r}) \equiv \left[-\frac{\hbar^2}{2m}\nabla^2 + V_{\text{eff}}(\mathbf{r}) \right]\psi_i(\mathbf{r}) = \varepsilon_i\psi_i(\mathbf{r}), \tag{2.5}$$

with

$$V_{\text{eff}}(\mathbf{r}) = V_C(\mathbf{r}) + V_{xc}(\mathbf{r}). \tag{2.6}$$

These equations are similar to a non-interacting single-particle Schrödinger equation, where i labels each electron in the system. However, the potential has been replaced by an effective potential V_{eff} consisting of two contributions: the electrostatic Coulomb potential of the interaction of all charges in the system,

$$V_C(\mathbf{r}) = \frac{e^2}{4\pi\epsilon_0}\int \frac{n(\mathbf{r}')}{|\mathbf{r}-\mathbf{r}'|}d^3r' - \frac{1}{4\pi\epsilon_0}\sum_I \frac{Ze^2}{|\mathbf{r}-\mathbf{R}_I|}, \tag{2.7}$$

and the exchange-correlation potential which is given by the functional derivative

$$V_{xc}(\mathbf{r}) = \frac{\delta E_{xc}[n(\mathbf{r})]}{\delta n(\mathbf{r})}. \tag{2.8}$$

Moreover, the ground-state density of this system is easily obtained from

$$n(\mathbf{r}) = \sum_i^{\text{occ}} |\psi_i(\mathbf{r})|^2, \tag{2.9}$$

where the single-particle wave function $\psi_i(\mathbf{r})$[1] are the solutions of the Kohn-Sham equations and the summation takes over all occupied one-electrons states.

To find the ground-state density, the second Hohenberg-Kohn theorem is no longer needed. One can calculate the density of an interacting (many-body) system in a potential by solving the equations of a non-interacting (single-body) system in an effective potential.

Since the effective potential V_{eff} depends on the density $n(\mathbf{r})$, which in turn depends on ψ_i, which in turn depend on V_{eff} and so on. This means that the KS equation must be *solved iteratively*. At the beginning, some starting density $n^{(0)}$ is guessed (it can be constructed by a superposition of atomic densities), and the potential $V^{(1)}$ is constructed with it. Then the Eq. (2.5) can be written down, and the eigenvalue is solved. This gives a set of $\psi^{(1)}$ from which a density $n^{(1)}$ can be derived by using Eq. (2.9). Now $n^{(1)}$ is used to construct a new better potential $V^{(2)}$, which will yield a $n^{(2)}$, etc. This procedure will be continued until the density converges to a density $n^{(f)}$, i.e., the self-consistency is achieved.

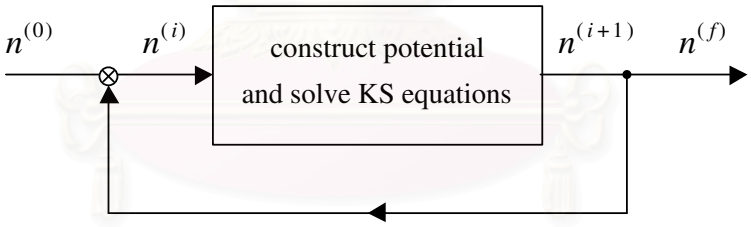

Figure 2.1: Schematic of the system for producing self-consistency

2.1.3 Local density approximation

The Kohn-Sham scheme described in the previous section is exact (apart from the preceding Born-Oppenheimer approximation), if the exchange correlation functional $E_{xc}[n]$ is known. Unfortunately, no exact functional of E_{xc} has been found yet. Thus, some approximations of E_{xc} must be used. The simplest method of

[1]Beware that the single-particle wave functions $\psi_i(\mathbf{r})$ are not the wave functions of electrons! They describe mathematical quasi-particles, without a direct physical meaning. Only the overall density of these quasi-particles is guaranteed to be equal to the true electon density.

describing the exchange-correlation energy of an electronic system is called the *local density approximation* (LDA).

In the LDA, the exchange-correlation energy is constructed by assuming that the exchange-correlation energy per electron at some position $\mathbf{r}$ is equal to the known exchange-correlation energy per electron of a *homogeneous electron gas* with the same density at the position $\mathbf{r}$. Thus, the approximate functional E_{xc} can be written as

$$E_{xc}[n(\mathbf{r})] = \int n(\mathbf{r})\varepsilon_{xc}(n(\mathbf{r}))d^3r, \tag{2.10}$$

and

$$\frac{\delta E_{xc}[n(\mathbf{r})]}{\delta n(\mathbf{r})} = \frac{\partial[n(\mathbf{r})\,\varepsilon_{xc}(n(\mathbf{r}))]}{\partial n(\mathbf{r})}, \tag{2.11}$$

with

$$\varepsilon_{xc}(n(\mathbf{r})) \equiv \varepsilon_{xc}^{homo}[n(\mathbf{r})]. \tag{2.12}$$

It is important to note that ε_{xc} is not a functional, but a function of $n(\mathbf{r})$ at a particular point of space. This local definition makes the KS equation easy to be solved. There exist many expressions for ε_{xc} based on various methods. The expression used in this work is proposed by Hedin-Lundqvist [16], that is

$$\varepsilon_{xc}(\mathbf{r}) = -\frac{3}{2}\left(\frac{3n(\mathbf{r})}{\pi}\right)^{1/3} - 0.045\left[\left(1+\frac{r_s}{21}\right)^3 \ln(1+\frac{21}{r_s}) + \frac{r_s}{2\cdot 21} - \left(\frac{r_s}{21}\right)^2 - \frac{1}{3}\right], \tag{2.13}$$

where r_s is defined as the radius of the sphere whose volume corresponds to the average volume per electron:

$$\frac{4\pi}{3}\, r_s^3 \;=\; n^{-1}\,. \tag{2.14}$$

The LDA is widely used and very successful. It performs well for systems with a slowly varying density. But rather surprisingly, it even works reasonably well in systems which the electron density is rapidly varying. It is possible to improve the correction of the exchange-correlation energy due to nearby inhomogeneities in the electron density. One obvious way is to make the exchange-correlation energy depend not only on the local value of the density, but on the extent to the gradient of the density. This form of approximation is therefore called the *generalized gradient approximation* (GGA). Recently, more sophisticated treatments of high correlated systems have been developed such as LDA+U. However, they are beyond the scope of our work.

2.2 Solutions of the single-particle Kohn-Sham equations

Consider the problem of finding the solution of the Kohn-Sham equations, the set of Eqs. (2.5) are solved to obtain the eigenvalues ε_i and corresponding eigenstates ψ_i for each of the electrons in the system. Instead of solving differential equations such as Eq. (2.5) directly, it is possible to determine the ground-state without the explicit solution of the Kohn-Sham equations. One way is to represent the solution in terms of the expansion of some known functions which are called *basis sets* and then try to find the coefficients in this expansion.

In the case of solids, the number of the equations is infinite, and each wave function must be calculated over the entire space of the solids. However, if the system is a perfect crystal, *Bloch's theorem* can be used to reduce the domain of the problem to one unit cell, and it transforms the problem into *k-space* in which the number of calculated states can be finite. (This will be discussed in Section 3.4.1.) Thus, for solids, it is almost the case that expanding the wave function ψ in a set of basis functions which satisfy Bloch's condition.

The wave functions are now labelled with band index ν and wave vector $\mathbf{k}$ and written as linear combination of defined basis functions $\phi_{\mathbf{G}}$ as

$$\psi_\nu(\mathbf{k},\mathbf{r}) = \sum_{\mathbf{G}} c^\nu_{\mathbf{G}}(\mathbf{k})\,\phi_{\mathbf{G}}(\mathbf{k},\mathbf{r}), \tag{2.15}$$

where $c^\nu_{\mathbf{G}}(\mathbf{k})$ are (as yet unknown) the expansion coefficients. The sum of basis functions is performed over reciprocal lattice vectors $\mathbf{G}$. In principle, the number of $\mathbf{G}$ in the summation is infinite, but in practice it must be truncated to a finite value. Such a limited basis set will never be able to describe $\psi_\nu(\mathbf{k},\mathbf{r})$ exactly. However, if the number of the included basis functions is large enough, this can generate a function close to $\psi_\nu(\mathbf{k},\mathbf{r})$.

Given a basis set, the Kohn-Sham eigenvalues and eigenstates can be determined by the *Rayleigh-Ritz variational method*. This leads to a generalized

eigenvalue problem:

$$\begin{bmatrix} \cdots & \cdots & \cdots \\ \vdots & H_{\mathbf{GG'}} - \varepsilon_\nu S_{\mathbf{GG'}} & \vdots \\ \cdots & \cdots & \cdots \end{bmatrix} \begin{bmatrix} c_1^\nu \\ \vdots \\ c_N^\nu \end{bmatrix} = \begin{bmatrix} 0 \\ \vdots \\ 0 \end{bmatrix}, \quad \text{for each } \mathbf{k}, \tag{2.16}$$

where the matrix elements of the Hamiltonian $H_{\mathbf{GG'}}$ and the overlap matrix $S_{\mathbf{GG'}}$ are given as

$$H_{\mathbf{GG'}}(\mathbf{k}) = \int \phi^*_{\mathbf{G}}(\mathbf{k},\mathbf{r})\, \hat{H}_{KS}\, \phi_{\mathbf{G'}}(\mathbf{k},\mathbf{r})\, d^3r, \tag{2.17}$$

and

$$S_{\mathbf{GG'}}(\mathbf{k}) = \int \phi^*_{\mathbf{G}}(\mathbf{k},\mathbf{r})\, \phi_{\mathbf{G'}}(\mathbf{k},\mathbf{r})\, d^3r. \tag{2.18}$$

The size of the square matrix $\mathbf{H}$ and $\mathbf{S}$ is equal to the number of basis functions, N, which is determined by the choice of a cutoff parameter G_{max}. That is, all reciprocal lattice vectors taken into the basis set are smaller than this cutoff, i.e., $\|\mathbf{G}\| \leq G_{max}$. Diagonalization will yield N eigenvalues, ε_ν, and N sets of coefficients, c^ν, that characterize each of the N eigenfunctions, ψ_ν. Note that the matrix is a function of the wave vector $\mathbf{k}$. The discrete set of $\varepsilon_\nu(\mathbf{k})$ and corresponding $\psi_\nu(\mathbf{k})$ that we have found in one diagonalization will be the eigenvalues and eigenfunctions for a particular state $\mathbf{k}$ but for a different index ν. Therefore, Eq. (2.16) has to be calculated independently for each of point $\mathbf{k}$ in the first Brillioun zone.

An optimal choice of the basis set is one in which the number of basis functions needed to express the desired solutions is as small as possible. This ensures that the size of matrix to be solved is small; also, it helps to save the computing time. If the functions of the basis set are very similar to ψ, one needs only a few of them to accurately describe the wave functions. Such a basis set is called *efficient*. However, it must not bias too much to the solutions. The art of computational solid state physics is to construct sophisticated basis functions which provide a good approximation to the true solution. Each such basis generates its own specific technical demands, hence each has its own name of method.

2.3 The FLAPW method

This section describes the full-potential linearized augmented-plane-wave (FLAPW) method that we have used to solve the Kohn-Sham equations for a general charge

density and potential. The subject is arranged in order of complication.

2.3.1 PW

A natural basis set for calculating the single-particle wave functions in a periodic solid is the plane wave (PW) basis set. The use of this basis set has several advantages: it makes most algebraic manipulations very simple, and the fast Fourier transform algorithm can be adopted. However, since the electron wave functions oscillate rapidly near the core, a large number of plane waves are needed to accurately describe the wave functions in the core region. This makes plane waves very inefficient.

In order to overcome this problem one can employ a *pseudopotential*, which eliminates these rapid oscillations, due to the core electrons, by replacing the potential with a weaker (pseudo)potential that yields smooth tails of the wave functions in the core region. As a result, fewer plane waves are needed. The pseudopotential plane wave method is widely successful implementation because the valence electrons are much greater significant to physical properties than the core electrons, but it is poorly suited for the system involving with the core electrons or the wave functions near the nucleus such as transition metals and first-row elements. Another way to solve this problem is to use atomic-like functions to describe the wave functions near the core, as done in the augmented-plane-wave method [17].

2.3.2 APW

The *augmented-plane-wave* (APW) has been introduced by Slater [18] as a basis set for solving the one electron equations, which correspond to the Kohn-Sham equations within DFT. The APW method is based on an approximate model of the potential in a specific crystal. At regions near each nucleus, the potential is expected to be rather spherical symmetric and in regions between the nuclei it is expected to be relatively flat. The actual potential will be approximated to have a *muffin-tin* form, which means that within a unit cell the potential is assumed to be spherically symmetric inside a non-overlapping sphere around each nucleus,

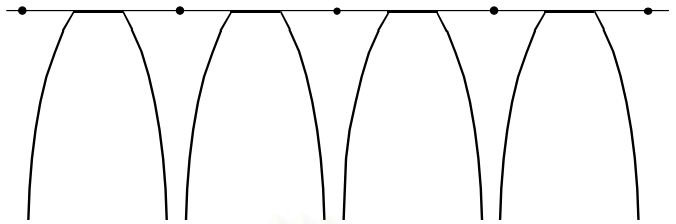

(a)

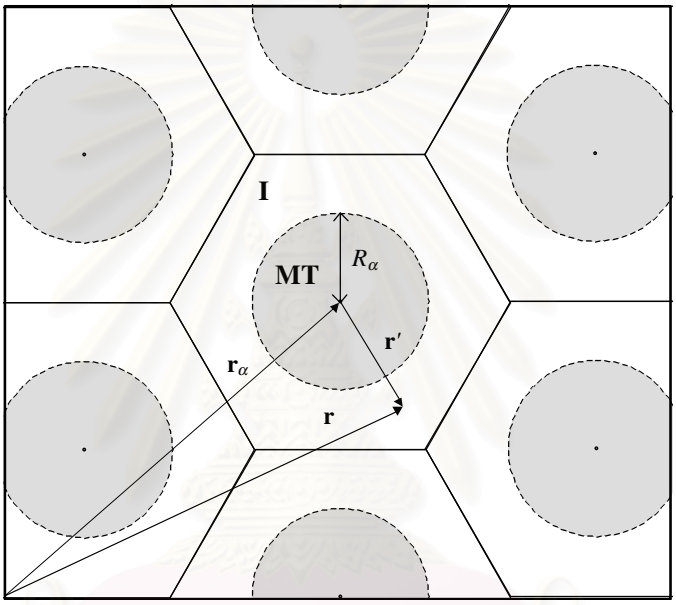

(b)

Figure 2.2: (a) The muffin-tin potential, plotted along a line of ions. (b) Division of a unit cell in muffin-tin regions and the interstitial region.

the so-called muffin-tin (MT) sphere, and set to be constant in the remaining interstitial (I) region, (see Fig. 2.2). In view of the choice of the potential, an APW basis function used in the expansion of the single-particle wave functions in a unit cell is defined as:

$$\phi_{\mathbf{G}}(\mathbf{k},\mathbf{r}) = \begin{cases} \frac{1}{\sqrt{\Omega}}\, \mathrm{e}^{i(\mathbf{k}+\mathbf{G})\cdot\mathbf{r}} & : \mathbf{r} \in \mathrm{I} \\ \displaystyle\sum_{\ell m} A^{\alpha}_{\ell m}\, u^{\alpha}_{\ell}(r', E)\, Y_{\ell m}(\hat{\mathbf{r}}') & : \mathbf{r} \in \mathrm{MT}_{\alpha}\ , \end{cases} \tag{2.19}$$

where the symbols $\mathbf{k}$ and $\mathbf{G}$ keep their usual meaning. Ω is the volume of the unit cell, α indexes the different spheres in the unit cell, and $\mathbf{r}' = \mathbf{r} - \mathbf{r}_\alpha$ is the position inside the spheres given with respect to the center of each sphere. Strictly

speaking, the APW basis consists of a plane wave in space outside the sphere and a linear combination of radial functions u_ℓ times spherical harmonics $Y_{\ell m}$, with which the plane wave is augmented, inside the muffin-tin sphere α of radius R_α. $u_\ell^\alpha(r', E)$ is the regular solution of the radial Schrödinger equation for the energy E and also the spherical part of the potential inside sphere α. It is constructed by integrating the equation

$$\left[-\frac{\hbar^2}{2m}\frac{\partial^2}{\partial r'^2} + \frac{\hbar^2}{2m}\frac{\ell(\ell+1)}{r'^2} + V(r') - E\right] r' u_\ell = 0. \tag{2.20}$$

The coefficients $A_{\ell m}$ are a function of $\mathbf{k}+\mathbf{G}$ and determined by requiring that the function inside the sphere matches (in value) with the plane wave at the boundary of muffin-tin spheres. Notice that an APW is a continuous function, but there is a discontinuity in its slope at the surface of the sphere. Here $\sum_{\ell m}$ means $\sum_{\ell=0}^{\infty}\sum_{m=-\ell}^{\ell}$. In practice we will have to truncate this sum to some value ℓ_{max}.[2] The number of ℓ-values to be included in the summation is arbitrary at this point, but we shall certainly want to include all the lower values ($\ell = 0, 1, 2, 3$) in order to represent any s, p, d or f character in the wave functions.

Unfortunately, the APW basis will not offer enough variational freedom, if the nonlinear energy parameter E used in setting up the radial solutions is set to an arbitrary value. It turns out that in order to describe $\psi_\nu(\mathbf{k})$ accurately with the APW basis set, one has to set E equal to the energy eigenvalue (or band energy) $\varepsilon_\nu(\mathbf{k})$ of that state. But this is exactly what we are searching for. This makes the APW basis functions *energy dependent*. The matrix representations in such a basis set will, of course, also be energy dependent.

This energy dependence causes two significant computational difficulties. First, it leads to a *non-linear* eigenvalue problem, which a lot of computations are demanded for solving it. The way to find the eigenvalues is to find the energies that correspond to a zero of the determinant $|\mathbf{H} - E\mathbf{S}|$. This makes it necessary to plot these determinants (see Fig. 2.3). This procedure consumes a lot of computer power and makes the method quite slow. The second is that the APW secular equation exhibits singularities whenever a node of the radial solution falls on a MT sphere boundary, i.e., $u_\ell(R_\alpha, E) = 0$. These difficulties limit the use of the APW method.

[2]Typically, $\ell_{max} = 8$ is sufficient for most simple systems with cubic symmetry.

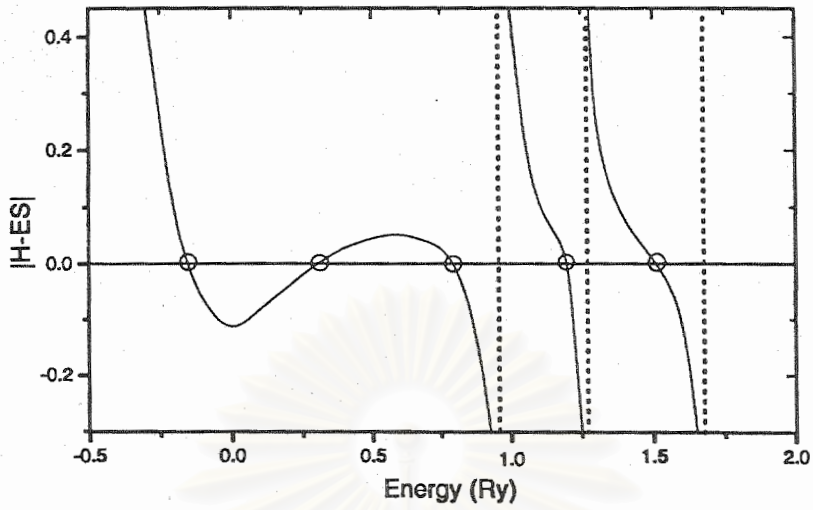

Figure 2.3: A suggestive visualization of how the roots of the secular equation are searched. (picture reproduced from K. Schwarz et al., *Computer Physics Communications*, 147 (2002) pp.71)

2.3.3 LAPW

Several improvements to solve the energy dependence of the basis set have been tried, but the first really successful one was the linearized scheme introduced by Andersen [19]. Koelling and Arbman [20] then took up the concept and refined it, leading to the *linearized augmented-plane-wave* (LAPW) method [21]. The basic idea of the LAPW method is to add an extra variational freedom to the basis inside the MT sphere, so that it is not necessary to set the energy parameter E equal to $\varepsilon_{\nu\mathbf{k}}$. This is done by using not only the radial solution of the Schrödinger equation, but its derivative with respect to the energy as well. To illustrate, if we have calculated u_ℓ at some energy E_0, we could make a Taylor expansion to find u_ℓ at energies not far away from it:

$$u_\ell(r', \varepsilon_{\nu\mathbf{k}}) = u_\ell(r', E_0) + (E_0 - \varepsilon_{\nu\mathbf{k}}) \left.\frac{\partial u_\ell(r', E)}{\partial E}\right|_{E=E_0} + O(E_0 - \varepsilon_{\nu\mathbf{k}})^2. \qquad (2.21)$$

Then we substitute the first two terms of the expansion in the APW for a fixed E_0 and introduce an undetermined coefficient B_{lm} for the unknown energy difference $(E_0 - \varepsilon_{\nu\mathbf{k}})$. This gives the definition of an LAPW basis function in the following

form:

$$\phi_{\mathbf{G}}(\mathbf{k},\mathbf{r}) = \begin{cases} \frac{1}{\sqrt{\Omega}}\, \mathrm{e}^{i(\mathbf{k}+\mathbf{G})\cdot\mathbf{r}} & : \mathbf{r} \in \mathrm{I} \\ \sum\limits_{\ell m} \left[A^{\alpha}_{\ell m} u^{\alpha}_{\ell}(r', E_0) + B^{\alpha}_{\ell m} \dot{u}^{\alpha}_{\ell}(r', E_0)\right] Y_{\ell m}(\hat{\mathbf{r}}') & : \mathbf{r} \in \mathrm{MT}_{\alpha}\ , \end{cases} \tag{2.22}$$

where $\dot{u}_\ell$, which appears in the LAPW but not the APW, denotes the energy derivative of u_ℓ. The coefficient $A_{\ell m}$ and $B_{\ell m}$ are determined by requiring that the function in the sphere matches the plane wave both in value and in slope at the sphere boundary.

As with the original APW basis, the radial function $u_\ell(r', E_0)$ is obtained by numerical integrating Eq. (2.20), while $\dot{u}_\ell(r', E_0)$ is obtained from

$$\left[-\frac{\hbar^2}{2m}\frac{\partial^2}{\partial r'^2} + \frac{\hbar^2}{2m}\frac{\ell(\ell+1)}{r'^2} + V(r') - E_0\right] r'\dot{u}_\ell = r' u_\ell. \tag{2.23}$$

The above equation is derived by taking the energy derivative of Eq. (2.20) directly. It will be useful to require the radial solutions to be normalized inside the MT sphere:

$$\int_0^{R_\alpha} u_\ell^2\, r^2 dr = 1. \tag{2.24}$$

By differentiating this normalization condition with respect to the energy, we see immediately that $\dot{u}_\ell$ and u_ℓ are orthogonal. However, $\dot{u}_\ell$ is not in general normalized inside the MT sphere.

In contrast to the APW formalism, the energy parameter is now kept *fixed* to a linearization energy, E_0, and the LAPW basis functions are flexible enough to represent all eigenfunctions in an energy range around this linearization energy. However, the radial function itself has an error of order $(E_0 - \varepsilon_{\nu\mathbf{k}})^2$, and there will be an error of order $(E_0 - \varepsilon_{\nu\mathbf{k}})^4$ in the energy eigenvalue. It is therefore beneficial to choose E_0 near the center of the interested bands. Note that the method permits different choices of the energy parameter for different angular momenta, ℓ. Thus, instead of choosing a single universal E_0, one could choose a set of E_ℓ for each ℓ-character of bands. For example, $E_{\ell=0}$ will be set to be roughly in the middle of s-band, $E_{\ell=1}$ in the middle of p-band, and similarly for every physically important ℓ (s-, p-, d- and f-bands, i.e. up to $\ell = 3$). For higher ℓ, a fixed value could be applied.

In the LAPW method the energy dependent has been removed, so it is an easy task to find all eigenvalues by simply diagonalizing the secular matrix just once. The cost of the energy-independent LAPW basis set is an increased number of basis functions. Recently, an new alternative way of linearizing, namely APW+lo [22, 23], has been proposed, which still has the same size as in the APW method. It is beyond scope of our work. Another advantage of the LAPW method is that it can be extended to include the entire potential, the so-called non-muffin-tin potential, with a little difficulty.

2.3.4 The full-potential

In the APW and LAPW method, the muffin-tin approximation is applied to the potential used in the Hamiltonian. The LAPW method, however, enables us to correct the potential by including the non-muffin-tin effects. This can be done by writing the potential in the form:

$$V(\mathbf{r}) = \begin{cases} \sum_{\mathbf{G}} V_{\mathbf{G}}\, \mathrm{e}^{i\,\mathbf{G}\cdot\mathbf{r}} & : \mathbf{r} \in \mathrm{I} \\ \sum_{\ell m} V_{\ell m}(r')\, Y_{\ell m}(\hat{\mathbf{r}}') & : \mathbf{r} \in \mathrm{MT}. \end{cases} \tag{2.25}$$

That is, the potential in the interstitial region is expressed as a Fourier series, and the potential inside the MT spheres is expanded in terms of spherical harmonics. (The muffin-tin approximation corresponds to retaining only the $\ell = m = 0$ component inside the spheres and only $\mathbf{G} = 0$ component outside.) This form of potential is completely general; thus no shape approximation is introduced and therefore such an approach is called a *full-potential* treatment. Likewise, the electron density (and also the charge density) is represented in the same way as the potential:

$$n(\mathbf{r}) = \begin{cases} \sum_{\mathbf{G}} n_{\mathbf{G}}\, \mathrm{e}^{i\,\mathbf{G}\cdot\mathbf{r}} & : \mathbf{r} \in \mathrm{I} \\ \sum_{\ell m} n_{\ell m}(r')\, Y_{\ell m}(\hat{\mathbf{r}}') & : \mathbf{r} \in \mathrm{MT}. \end{cases} \tag{2.26}$$

The Coulomb potential is determined from the charge density via Poisson's equation. With this representation of the density and the potential, one technique called the *pseudocharge* method is usually used for obtaining the solution of the

Poisson's equation. The detail of solving Poisson's equation without the shape approximation for arbitrarily charge distribution is described in Section 3.6.1.

2.4 The total energy

The structural properties of solids are studied primarily through comparisons of total energies between different crystal structures, volumes and atomic positions. This requires calculations of the total energy as a function of the arrangement of atoms. In these calculations, the nuclei are considered to be at rest at lattice sites; hence, this corresponds to the temperature at 0 K. Nevertheless, the quantum mechanics of vibrations demands that the ground state can never have the atoms completely at rest. This is the so-called *zero point motions*. However, for many properties the effects of lattice dynamics are less significant, and the neglect of dynamics can be justified as a reasonable compromise.

Within the density functional framework, the total energy of a solid for a particular configuration of the ions is given by

$$E_{tot} \;=\; T_s \;+\; U_{ee} \;+\; U_{ne} \;+\; E_{xc} \;+\; U_{nn}. \tag{2.27}$$

As discussed in Section 2.1.2 we express the total energy of the electrons as a sum of the kinetic energy of the non-interacting electrons, the potential energy due to the Coulomb interaction of the electron-electron, U_{ee}, and the electron-nuclear, U_{ne}, and the exchange-correlation energy, E_{xc}. In addition, the Coulomb interactions of the atomic nuclei, U_{nn}, the so-called *Madelung energy*, has to be taken into account. The kinetic energy per unit cell can be calculated reliably by making explicit use of the Khon-Sham equations; then a simple expression of the kinetic energy term is

$$\begin{aligned} T_s &= \sum_{\nu\mathbf{k}} \int \psi^*_{\nu\mathbf{k}} \Big(-\frac{\hbar^2}{2m}\nabla^2 \Big) \psi_{\nu\mathbf{k}} \, d^3r \\ &= \sum_{\nu\mathbf{k}} \varepsilon_{\nu\mathbf{k}} - \int_\Omega V_{\text{eff}}(\mathbf{r})\, n(\mathbf{r})\, d^3r, \end{aligned} \tag{2.28}$$

where $\varepsilon_{\nu\mathbf{k}}$ and $n(\mathbf{r})$ are the energy eigenvalues and the electron density obtained from the solutions of the KS equations with the summation running over all the

occupied states. The interaction energy between all charges in the system is summarized as the potential energy U:

$$U \;=\; \frac{e^2}{8\pi\epsilon_0}\left[\iint \frac{n(\mathbf{r})n(\mathbf{r}')}{|\mathbf{r}-\mathbf{r}'|}\,d^3r\,d^3r' \;-\; 2\sum_I Z_I\int\frac{n(\mathbf{r})}{|\mathbf{r}-\mathbf{R}_I|}\,d^3r \;+\; \sum_{I\neq J}\frac{e^2Z_IZ_J}{|\,\mathbf{R}_I-\mathbf{R}_J|}\right], \tag{2.29}$$

where $\sum_I$ is over the nuclei. Since the Coulomb potential at $\mathbf{r}$ is given by Eq. (2.7), the potential energy per unit cell becomes

$$U = \frac{1}{2}\left[\int_\Omega n(\mathbf{r})\,V_C(\mathbf{r})\,d^3r - \sum_\alpha Z_\alpha V_M(\mathbf{r}_\alpha)\right], \tag{2.30}$$

where the sum on α runs over the nuclei at $\mathbf{r}_\alpha$ in the unit cell. We have defined a generalized Madelung potential $V_M(\mathbf{r}_\alpha)$ as

$$V_M(\mathbf{r}_\alpha) = \frac{e^2}{4\pi\epsilon_0}\left(\int\frac{n(\mathbf{r})}{|\mathbf{r}-\mathbf{r}_\alpha|}\,d^3r \;-\; \sum_{I\neq\alpha}\frac{Z_I}{|\mathbf{R}_I-\mathbf{r}_\alpha|}\right), \tag{2.31}$$

i.e., the Coulomb potential at $\mathbf{r}_\alpha$ due to all charges in the crystal except for the nucleus at this site. The exchange-correlation energy is given directly by its definition in the local density approximation as in Eq. (2.10). By collecting all terms, the total energy per unit cell can be rewritten as

$$\begin{aligned} E_{tot} \;&=\; \sum_{\nu\mathbf{k}}\varepsilon_{\nu\mathbf{k}} \;-\; \frac{1}{2}\sum_\alpha Z_\alpha V_M(\mathbf{r}_\alpha) \\ &\quad - \int_\Omega n(\mathbf{r})\left[\,\frac{1}{2}V_C(\mathbf{r}) \;+\; V_{xc}(\mathbf{r}) \;-\; \varepsilon_{xc}(\mathbf{r})\,\right]d^3r. \end{aligned} \tag{2.32}$$

The above equation will hold exactly the total energy only for the self-consistent electron density. During the iterations on the way to self-consistency, this result represents only an approximation to the total energy.

The major problem in evaluating the total-energy expression involves the necessity of numerical cancellation of the very large (positive) kinetic and large (negative) potential energy contributions. As is well known, there will be an error when a subtraction between large numbers is performed. This subtraction error causes the numerical instability to the value of the total energies. A successful solution for this problem has been presented by Weinert, Wimmer and Freeman [4]. The key feature is the explicit *algebraic* cancellation of the Coulomb singularities

in the kinetic and potential energy terms by using the new form of generalized Madelung potential. We have implemented their formalism in our total-energy calculations, which leads to good numerical stability of our results.

Chapter 3

Calculation Details

3.1 Determination of $A_{\ell m}$ and $B_{\ell m}$ coefficients

Within the LAPW method the electron wave functions are expanded differently in two types of regions, plane waves in the interstitial region and a linear combination of spherical solutions in the muffin-tin. The arbitrary expansion coefficients $A_{\ell m}$ and $B_{\ell m}$ will be specified from the requirement that the basis functions and their derivatives are continuous across the sphere boundaries. This is accomplished by matching the functions inside and outside the sphere of each basis both in value and in derivative at the MT sphere boundary.

Consider the form of plane wave solutions in the vicinity of the αth sphere. In the local coordinate frame this can be written as

$$\mathrm{e}^{i(\mathbf{k}+\mathbf{G})\cdot\mathbf{r}} \;=\; \mathrm{e}^{i(\mathbf{k}+\mathbf{G})\cdot(\mathbf{r}_\alpha+\mathbf{r}')} \;=\; \mathrm{e}^{i(\mathbf{k}+\mathbf{G})\cdot\mathbf{r}_\alpha}\,\mathrm{e}^{i(\mathbf{k}+\mathbf{G})\cdot\mathbf{r}'}. \tag{3.1}$$

(For one sphere in the unit cell we can take $\mathbf{r}_\alpha = 0$.) By using the *Rayleigh expansion*, a plane wave can be expanded in spherical harmonics as

$$\mathrm{e}^{i\mathbf{k}\cdot\mathbf{r}} = 4\pi \sum_{\ell m} i^\ell j_\ell(kr)\, Y^*_{\ell m}(\hat{\mathbf{k}}) Y_{\ell m}(\hat{\mathbf{r}}). \tag{3.2}$$

Thus Eq. (3.1) becomes

$$\mathrm{e}^{i\mathbf{k_G}\cdot\mathbf{r}} = 4\pi\, \mathrm{e}^{i\mathbf{k_G}\cdot\mathbf{r}_\alpha} \sum_{\ell m} i^\ell j_\ell(k_{\mathbf{G}} r')\, Y^*_{\ell m}(\hat{\mathbf{k}}_{\mathbf{G}}) Y_{\ell m}(\hat{\mathbf{r}}'), \tag{3.3}$$

where

$$\mathbf{k_G} \;\equiv\; \mathbf{k} + \mathbf{G}, \tag{3.4}$$

and $j_\ell(x)$ is the spherical Bessel function of order ℓ. Evaluating (3.3) at the surface of the αth sphere and equating value and slope to the functions inside the sphere, this leads to the 2×2 linear equations:

$$A_L\, u_\ell(R_\alpha) + B_L\, \dot{u}_\ell(R_\alpha) \;=\; \lambda\, j_\ell(k_{\mathbf{G}} R_\alpha), \tag{3.5a}$$

$$A_L\, u'_\ell(R_\alpha) + B_L\, \dot{u}'_\ell(R_\alpha) \;=\; \lambda\, j'_\ell(k_{\mathbf{G}} R_\alpha), \tag{3.5b}$$

with

$$\lambda \;=\; \mathrm{e}^{i\mathbf{k_G}\cdot\mathbf{r}_\alpha} \frac{4\pi}{\sqrt{\Omega}}\, i^\ell\, Y_L^*(\hat{\mathbf{k}}_{\mathbf{G}}), \tag{3.6}$$

where the prime denotes the derivative with respect to r', and L is the abbreviation of ℓm. Solving these equations for A_L and B_L yields

$$A_L^\alpha(\mathbf{k_G}) = \lambda\, R_\alpha^2 a_\ell^\alpha, \tag{3.7a}$$

$$a_\ell^\alpha = [\, j'_\ell(k_{\mathbf{G}} R_\alpha)\dot{u}_\ell(R_\alpha) - j_\ell(k_{\mathbf{G}} R_\alpha)\dot{u}'_\ell(R_\alpha)\,], \tag{3.7b}$$

$$B_L^\alpha(\mathbf{k_G}) = \lambda\, R_\alpha^2 b_\ell^\alpha, \tag{3.7c}$$

$$b_\ell^\alpha = [\, j_\ell(k_{\mathbf{G}} R_\alpha) u'_\ell(R_\alpha) - j'_\ell(k_{\mathbf{G}} R_\alpha) u_\ell(R_\alpha)\,], \tag{3.7d}$$

where we have used the relation

$$[\, u'_\ell(R_\alpha)\dot{u}_\ell(R_\alpha) - u_\ell(R_\alpha)\dot{u}'_\ell(R_\alpha)\,] = \frac{1}{R^2}, \tag{3.8}$$

to write the dominator of the solutions as $1/R^2$.

3.2 The radial solutions

The radial functions $u_\ell(r)$ are solutions of the radial Schrödinger equation in the spherically averaged crystal potential with the linearization energy E_ℓ, while the $\dot{u}_\ell(r)$ are the derivatives with respect to E_ℓ. They are determined by numerically integrating the radial Schrödinger equation in Eq. (3.9).

Before proceeding the calculations it is extremely advantageous to apply an appropriate system of units to the problem. We have employed the *atomic units* in our calculations. That means, the unit of energy is the Rydberg energy, $me^4/2\hbar^2$, and the unit of length is the Bohr radius, $\hbar^2/me^2$. In this system of units one can verify that

$$\hbar = 1, \qquad m = \frac{1}{2}, \qquad e^2 = 2.$$

Now we can obtain the radial solutions $u_\ell(r)$ by solving the equation

$$-\frac{1}{r^2}\frac{\partial}{\partial r}r^2\frac{\partial u_\ell}{\partial r} \; + \; \left(\frac{\ell(\ell+1)}{r^2} \; + \; V(r)\right)u_\ell = E_\ell \, u_\ell. \tag{3.9}$$

The only boundary condition which must be imposed at this stage is that the radial solutions is regular at the origin without specifying the boundary condition at another end. For numerical integration of Eq. (3.9) it is convenient to change the independent variable r into logarithmic scale, i.e.,

$$x = \ln(r),$$

because it smoothly expands the radial scale near the origin where the wave function generally varies rapidly. If we simultaneously introduce the dependent function

$$W = \sqrt{r}\, u,$$

then the radial equation (3.9) becomes

$$W''(x) \; = \; \gamma \, W(x), \tag{3.10}$$

with

$$\gamma \; = \; \mathrm{e}^{2x}(V - E_\ell) \; + \; (\ell + \frac{1}{2})^2. \tag{3.11}$$

This form of the differential equation has the advantages that no first derivative is present and that $\ell = 0$ does not require any special treatment. In order to find the solutions of the Eq. (3.10), we have used the *Numerov method* [24]. In this method, numerical integrating is performed on a grid, outwardly from some starting point x_0 to the x_N corresponding to the sphere radius. By specifying some initial values, the method can predict the values at the preceding grid points and hence gives us the solutions.

It is necessary to have the first two values of W from which the integration starts. Since the origin of the radial coordinate ($r = 0$) corresponds to that $x \to -\infty$, in such a limit we have

$$\mathrm{e}^{2x}(V - E_\ell) \; \ll \; (\ell + \frac{1}{2})^2. \tag{3.12}$$

Consequently, the first term in Eq. (3.11) can be neglected. Thus for r close to zero, the differential equation (3.10) becomes

$$W'' \; = \; (\ell + \frac{1}{2})^2 \, W, \tag{3.13}$$

which has the solutions

$$W(x) = W(x_0)\,\mathrm{e}^{\pm(\ell+\frac{1}{2})(x-x_0)}. \tag{3.14}$$

The boundary condition that W is regular at the origin of radial coordinate eliminates the solution with the negative sign, and x_0 is chosen as some large negative number (e.g. -10) such that (3.12) is satisfied. Eq. (3.14) can be used to calculate the value of $W(x_1)$ based on the value of $W(x_0)$, and then the Numerov method can do the rest. Note that $W(x_0)$ can be set to any arbitrary value because we can have the true (absolute) values of W later by using the normalization condition.

For the radial solutions $\dot{u}_\ell(r)$ they are determined from the equation

$$-\frac{1}{r^2}\frac{\partial}{\partial r}r^2\frac{\partial \dot{u}_\ell}{\partial r} + \left(\frac{\ell(\ell+1)}{r^2} + V(r)\right)\dot{u}_\ell = E_\ell\,\dot{u}_\ell + u_\ell. \tag{3.15}$$

Transforming to the independent variable $x = \ln(r)$ again and putting $\dot{W} = \sqrt{r}\,\dot{u}$, this becomes

$$\dot{W}''(x) \;=\; \gamma\,\dot{W}(x) - \mathrm{e}^{2x}W(x), \tag{3.16}$$

which is an inhomogeneous differential equation. In the same way, Eq. (3.16) can be solved by using the Numerov method. The solution we get will be the particular solution, called W_p, while the homogeneous solution is exactly the same as the solution of Eq. (3.10). So the general solution of the Eq. (3.16) is

$$\dot{W} = c\,W + W_p, \tag{3.17}$$

where the constant c can be obtained from the orthogonal condition of u and $\dot{u}$.

3.3 Construction of the Hamiltonian matrix

The Hamiltonian matrix elements and the overlap matrix elements are given by Eqs. (2.17) and (2.18) respectively. In the following we will describe the way to evaluate them within the FLAPW method. Again, the calculations are performed in Rydberg atomic units.

Due to the different character of the basis functions in the different regions, the Hamiltonian and the overlap matrix will be constructed separately in the MT

and interstitial regions. Therefore, the volume integrations which are over the portion of the unit cell are divided into the interstitial part and the MT sphere part:

$$\int_{\Omega} \Longrightarrow \int_{\mathrm{I}} + \int_{\mathrm{MT}} \ .$$

The contribution of the interstitial part is given by

$$\begin{aligned} H^{\mathrm{I}}_{\mathbf{G}\mathbf{G}'} &= \frac{1}{\Omega} \int_{\mathrm{I}} \mathrm{e}^{-i(\mathbf{k}+\mathbf{G})\cdot\mathbf{r}} \left(-\nabla^2 + V(\mathbf{r})\right) \mathrm{e}^{i(\mathbf{k}+\mathbf{G}')\cdot\mathbf{r}} d^3r \\ &= \frac{1}{\Omega} \left\|\mathbf{k}+\mathbf{G}'\right\|^2 \int_{\mathrm{I}} \mathrm{e}^{-i(\mathbf{G}-\mathbf{G}')\cdot\mathbf{r}} d^3r \ + \ \frac{1}{\Omega} \int_{\mathrm{I}} V(\mathbf{r})\, \mathrm{e}^{-i(\mathbf{G}-\mathbf{G}')\cdot\mathbf{r}} d^3r. \end{aligned} \tag{3.18}$$

In practice, the integrations over the interstitial region are not straightforward to calculate because of the complicated structure of the interstitial region. An easy way to evaluate this is to extend the integral throughout the entire unit cell and subtract the contribution which results from the region inside the spheres. Let us now consider the integral of the form as in the first term of Eq. (3.18):

$$\begin{aligned} \Theta_{\mathbf{G}} &\equiv \frac{1}{\Omega} \int_{\mathrm{I}} \mathrm{e}^{-i\mathbf{G}\cdot\mathbf{r}} d^3r \\ &= \frac{1}{\Omega} \int_{\Omega} \mathrm{e}^{-i\mathbf{G}\cdot\mathbf{r}} d^3r \ - \ \frac{1}{\Omega} \sum_{\alpha} \int_{\mathrm{MT}_\alpha} \mathrm{e}^{-i\mathbf{G}\cdot\mathbf{r}} d^3r. \end{aligned} \tag{3.19}$$

The first term of (3.19) is simply the Dirac delta function (see Appendix D in Aschroft and Mermin, *Solid State Physics*). For the second term, using the local coordinates we have

$$\frac{1}{\Omega} \sum_{\alpha} \int_{\mathrm{MT}_\alpha} \mathrm{e}^{-i\mathbf{G}\cdot\mathbf{r}} d^3r = \frac{2\pi}{\Omega} \sum_{\alpha} \mathrm{e}^{-i\mathbf{G}\cdot\mathbf{r}_\alpha} \int_0^{R_\alpha} r'^2 dr' \int_0^{\pi} \sin\theta d\theta\, \mathrm{e}^{-iGr'\cos\theta}. \tag{3.20}$$

Thus

$$\Theta_{\mathbf{G}} = \delta_{\mathbf{G},0} - \sum_{\alpha} \mathrm{e}^{-i\mathbf{G}\cdot\mathbf{r}_\alpha} \frac{4\pi R_\alpha^3}{\Omega} \frac{j_1(GR_\alpha)}{GR_\alpha}, \tag{3.21}$$

where j_1 is the spherical Bessel function of order one. If we represent the potential in the interstitial region as in (2.25), we then have

$$\begin{aligned} \frac{1}{\Omega} \int_{\mathrm{I}} V(\mathbf{r})\, \mathrm{e}^{-i(\mathbf{G}-\mathbf{G}')\cdot\mathbf{r}} d^3r &= \sum_{\mathbf{G}''} V_{\mathbf{G}''} \frac{1}{\Omega} \int_{\mathrm{I}} \mathrm{e}^{-i(\mathbf{G}-\mathbf{G}'-\mathbf{G}'')\cdot\mathbf{r}} d^3r \\ &= \sum_{\mathbf{G}''} V_{\mathbf{G}''} \Theta_{(\mathbf{G}-\mathbf{G}'-\mathbf{G}'')}. \end{aligned} \tag{3.22}$$

Summarizing up to this point, the interstitial contributions to the Hamiltonian and the overlap matrix have the following form:

$$H^{\mathrm{I}}_{\mathbf{G}\mathbf{G}'} \;=\; \|\mathbf{k}+\mathbf{G}'\|^2\,\Theta_{(\mathbf{G}-\mathbf{G}')} \;+\; \sum_{\mathbf{G}''} V_{\mathbf{G}''}\Theta_{(\mathbf{G}-\mathbf{G}'-\mathbf{G}'')}, \tag{3.23}$$

and

$$S^{\mathrm{I}}_{\mathbf{G}\mathbf{G}'} = \Theta_{(\mathbf{G}-\mathbf{G}')}. \tag{3.24}$$

Note that $\sum_{\mathbf{G}'} V_{\mathbf{G}'}\Theta_{(\mathbf{G}-\mathbf{G}')}$ is a *discrete convolution*. To compute this, we used the fast Fourier transform (FFT) technique, because it is more efficient than computing it directly. A step-by-step of computing the convolution by using the FFT is shown in the figure below.

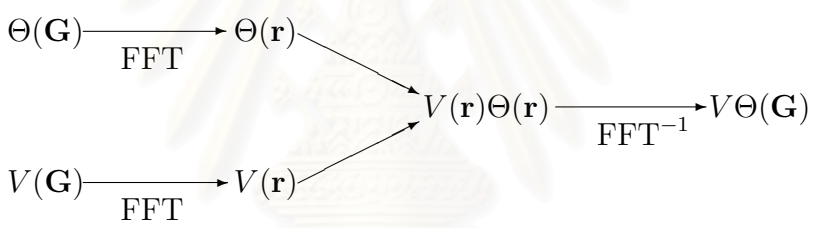

1. Obtain $\Theta(\mathbf{G})$ from Eq. (3.21) and $V(\mathbf{G})$ from the coefficients of the Fourier expansion of the potential
2. Use the FFT algorithm to compute the three dimensional discrete Fourier transform of Θ and of V
3. Multiply the two transforms together component by component
4. Use the FFT algorithm to take the inverse discrete Fourier transform of the products and obtain the discrete convolution,

$$V\Theta(\mathbf{G}) = \sum_{\mathbf{G}'} V_{\mathbf{G}'}\Theta_{(\mathbf{G}-\mathbf{G}')}$$

Figure 3.1: Computation procedure for the FFT convolution

Next, we find the Hamiltonian and the overlap matrix elements from the interiors of the muffin-tin spheres. In this case we split up the Hamiltonian into

two parts:

$$\hat{H}^{\rm MT} = \hat{H}^0 + \hat{V}^{ns}, \tag{3.25}$$

where $\hat{H}^0$ is the Hamiltonian inside the sphere which contains only the spherically symmetric potential, and $\hat{V}^{ns}$ is the non-spherical correction. To begin with the spherical part; we find that

$$\begin{aligned} H^0_{\mathbf{G}\mathbf{G}'} &= \sum_\alpha \int_{\rm MT} \left[\sum_L (A^\alpha_L u^\alpha_\ell + B^\alpha_L \dot{u}^\alpha_\ell) Y_L \right]^* \hat{H}^0 \left[\sum_{L'} (A^\alpha_{L'} u^\alpha_{\ell'} + B^\alpha_{L'} \dot{u}^\alpha_{\ell'}) Y_{L'} \right] d^3r \\ &= \sum_\alpha \sum_{LL'} \int_0^{R_\alpha} dr' r'^2 (A^\alpha_L u^\alpha_\ell + B^\alpha_L \dot{u}^\alpha_\ell)^* \hat{h}_{\ell'} \, (A^\alpha_{L'} u^\alpha_{\ell'} + B^\alpha_{L'} \dot{u}^\alpha_{\ell'}) \, \delta_{LL'} \\ &= \sum_\alpha \sum_L \big(A^{\alpha *}_L A^\alpha_L \langle u^\alpha_\ell | \hat{h}_\ell | u^\alpha_\ell \rangle \; + \; A^{\alpha *}_L B^\alpha_L \langle u^\alpha_\ell | \hat{h}_\ell | \dot{u}^\alpha_\ell \rangle \; + \\ &\qquad B^{\alpha *}_L A^\alpha_L \langle \dot{u}^\alpha_\ell | \hat{h}_\ell | u^\alpha_\ell \rangle \; + \; B^{\alpha *}_L B^\alpha_L \langle \dot{u}^\alpha_\ell | \hat{h}_\ell | \dot{u}^\alpha_\ell \rangle \big), \end{aligned} \tag{3.26}$$

where

$$\langle u^\alpha_\ell | \hat{h}_\ell | u^\alpha_\ell \rangle \; = \int_0^{R_\alpha} dr' r'^2 u^{\alpha *}_\ell(r') \, \hat{h}_\ell \, u^\alpha_\ell(r'), \tag{3.27}$$

with similar expressions for the other combinations of u_ℓ and $\dot{u}_\ell$, and $\hat{h}_\ell$ is the radial part of the Schrödinger equation, in which the potential has only $\ell = 0$ term. Since the radial solutions u_ℓ and $\dot{u}_\ell$ already satisfy the Eqs. (3.9) and (3.15), with the use of the normalization condition, we obtain

$$\begin{aligned} H^0_{\mathbf{G}\mathbf{G}'} &= \sum_\alpha \sum_L (A^{\alpha *}_L A^\alpha_L \, E_\ell \; + \; B^{\alpha *}_L B^\alpha_L \, E_\ell \, N_\ell \; + \; A^{\alpha *}_L B^\alpha_L) \\ &= \sum_\alpha \mathrm{e}^{i(\mathbf{G}'-\mathbf{G})\cdot \mathbf{r}_\alpha} \frac{4\pi R^4_\alpha}{\Omega} \sum_\ell (2\ell+1) P_\ell(\hat{\mathbf{k}}_\mathbf{G} \cdot \hat{\mathbf{k}}_{\mathbf{G}'}) \times \\ &\quad \big[\, a_\ell(k_\mathbf{G}) a_\ell(k_{\mathbf{G}'}) E_\ell \; + \; b_\ell(k_\mathbf{G}) b_\ell(k_{\mathbf{G}'}) E_\ell N_\ell \; + \; a_\ell(k_\mathbf{G}) b_\ell(k_{\mathbf{G}'}) \, \big]. \end{aligned} \tag{3.28}$$

Similarly, the overlap matrix is given by

$$\begin{aligned} S^{\rm MT}_{\mathbf{G}\mathbf{G}'} &= \sum_\alpha \mathrm{e}^{i(\mathbf{G}'-\mathbf{G})\cdot \mathbf{r}_\alpha} \frac{4\pi R^4_\alpha}{\Omega} \sum_\ell (2\ell+1) P_\ell(\hat{\mathbf{k}}_\mathbf{G} \cdot \hat{\mathbf{k}}_{\mathbf{G}'}) \times \\ &\quad \big[\, a_\ell(k_\mathbf{G}) a_\ell(k_{\mathbf{G}'}) \; + \; b_\ell(k_\mathbf{G}) b_\ell(k_{\mathbf{G}'}) N_\ell \, \big]. \end{aligned} \tag{3.29}$$

In arriving at these results the *addition theorem* [25] has been used to obtain the Legendre polynomial P_ℓ in place of the sum on spherical harmonics.

The remaining non-spherical part of the potential is calculated as follows:

$$\begin{aligned} V^{ns}_{\mathbf{GG}'} &= \sum_{\alpha} \int_{\mathrm{MT}} \left[\sum_{L} (A^{\alpha}_{L} u^{\alpha}_{\ell} + B^{\alpha}_{L} \dot{u}^{\alpha}_{\ell}) Y_L \right]^{*} \sum_{L''\neq 0} V^{\alpha}_{L''} Y_{L''} \left[\sum_{L'} (A^{\alpha}_{L'} u^{\alpha}_{\ell'} + B^{\alpha}_{L'} \dot{u}^{\alpha}_{\ell'}) Y_{L'} \right] d^3r \\ &= \sum_{\alpha} \sum_{L L' L''} \big[A^{\alpha *}_{L} A^{\alpha}_{L'} \langle u^{\alpha}_{\ell} | V^{\alpha}_{L''} | u^{\alpha}_{\ell'} \rangle \; + \; A^{\alpha *}_{L} B^{\alpha}_{L'} \langle u^{\alpha}_{\ell} | V^{\alpha}_{L''} | \dot{u}^{\alpha}_{\ell'} \rangle \; + \\ &\qquad B^{\alpha *}_{L} A^{\alpha}_{L'} \langle \dot{u}^{\alpha}_{\ell} | V^{\alpha}_{L''} | u^{\alpha}_{\ell'} \rangle \; + \; B^{\alpha *}_{L} B^{\alpha}_{L'} \langle \dot{u}^{\alpha}_{\ell} | V^{\alpha}_{L''} | \dot{u}^{\alpha}_{\ell'} \rangle \big] \, \mathcal{G}(L, L', L''), \end{aligned} \tag{3.30}$$

where $\mathcal{G}$ is the integral of three spherical harmonics [26] called *Gaunt coefficient*, i.e.

$$\mathcal{G}(L, L', L'') = \int Y^{*}_{L}(\hat{\mathbf{r}}) Y_{L'}(\hat{\mathbf{r}}) Y_{L''}(\hat{\mathbf{r}}) \, d\hat{\mathbf{r}}, \tag{3.31}$$

and it can be written in terms of Clebsh-Gordan coefficients [27]. The selection rules implied in $\mathcal{G}$ greatly reduce the number of nonzero terms (e.g. for cubic crystals where $V_{\ell m}$ is nonzero only for $\ell = 4, 6, 8$, etc.) in the sum and as well as the cost of computational time. However, it still takes a lot of time (about 75% of overall calculation time) to evaluate this non-spherical part. Because the non-spherical correction is quite small for high symmetry systems, we will neglect this term.

3.4 Brillouin zone integration

For a periodic system, the wave vector $\mathbf{k}$ appears in the wave function by virtue of Bloch's theorem. Wave functions $\psi_{\nu}(\mathbf{k})$ and energy eigenvalues $\varepsilon_{\nu}(\mathbf{k})$, therefore, depend on a band index ν and the wave vector $\mathbf{k}$ belonging to the first Brillouin zone. Both the Hamiltonian and the overlap matrix have to be calculated at each of these $\mathbf{k}$. Many quantities of the crystal, such as the electron density, the total energy, etc. are calculated by summing the matrix elements

$$X_{\nu}(\mathbf{k}) = \langle \psi_{\nu}(\mathbf{k}) | \, X \, | \, \psi_{\nu}(\mathbf{k}) \rangle \tag{3.32}$$

over all occupied states as

$$\langle X \rangle = \sum_{\nu \mathbf{k}}^{\mathrm{occ}} X_{\nu}(\mathbf{k}). \tag{3.33}$$

Such calculations often in principle require a knowledge of the value of the function at each $\mathbf{k}$ point in the Brillouin zone.

3.4.1 k-point sampling

Electronic states are allowed only at a set of discrete **k** points determined by the boundary conditions applied to the bulk solid. The density of allowed **k** points is proportional to the volume of the solid. There are, in principle, an *infinite* number of **k** points at which the wave functions must be calculated. Moreover, since the set of **k** is dense, the summations of the occupied states **k** can be changed to the integration over the first Brillouin zone. Thus

$$\langle X \rangle = \frac{1}{V_{BZ}} \int_{BZ} \sum_{\nu} X_{\nu}(\mathbf{k})\, d^3k. \tag{3.34}$$

However, the wave functions at **k** points that are very close together will be almost identical. Hence it is possible to replace the wave functions over a region of **k** space by the wave functions at a single **k** point. In this sense the electronic states at only a finite number of **k** points are required in calculation of Eq. (3.34). For example, the matrix elements and the wave functions can be computed only for a k-mesh in the zone, while the other values are recovered by interpolation. The most common techniques to perform the integration over the Brillouin zone efficiently and accurately are *the special point method* and *the tetrahedron method*. These methods aim at obtaining sufficient accuracy in the calculations with restriction to a few number of **k** points.

In addition, because the first Brillouin zone is invariant under point group operations, it makes sense to divide the Brillouin zone into regions, called *irreducible zones*, that can be repeated under point group operations to fill out the complete Brillouin zone. Since each irreducible zone is a copy of all the others and has identical energy surfaces, it is only necessary to compute the energy eigenvalues for those **k** lying in such a zone.

3.4.2 The tetrahedron method

To perform Brillouin zone integration we used the improved tetrahedron method [28]. By using this method, one can easily obtain an accurate approximation for the electron density, the total energy and other quantities depending on the Brillouin zone integration.

In the tetrahedron scheme, the irreducible part is divided into equally volumed tetrahedra whose corners are at the nodes of regular mesh of points filled up exactly the irreducible volume. Eigenvalues and matrix elements are obtained for the **k** points at the corners of the tetrahedra. Finally, the integration is approximated as a weighted sum over irreducible **k**-points $\mathbf{k}_j$

$$\langle X \rangle = \sum_{j,\nu} X_\nu(\mathbf{k}_j)\, w_{\nu j}, \tag{3.35}$$

where the weights $w_{\nu j}$ are independent of the matrix elements $X_\nu(\mathbf{k})$ and are calculated only once for a given set of energy bands with the tetrahedron method. The integration weights are derived by integrating each tetrahedron analytically after linearly interpolating energy $\varepsilon_\nu(\mathbf{k})$ inside the tetrahedron with energies at the four corners. The details are given in the reference [28]. The magnitude of any error of the total energy due to inadequacy of the k-point sampling can always be reduced by using a denser set of **k** points. The computed total energy will converge as the density of **k** points increase, and the error due to the k-point sampling then approaches to zero. In practice, there will be an examination for the best k-point sampling, that is dense enough to provide a sufficient accurate results but not too large to waste the computational time.

Moreover, the tetrahedron method can be used to calculate the density of states and hence determine the Fermi level.

3.5 Construction of the electron density

In this section we will discuss the determination of the total electron density from the eigenfunctions. After the wave functions are determined from the diagonalization, the electron density is obtained by the usual expression, i.e. the absolute squared of the normalized wave function. To get the total electron density, the densities for all the states below the Fermi level are integrated. If we use the Brillouin zone integration method, the total electron density will be calculated as

$$n(\mathbf{r}) = 2 \sum_{\nu j} |\psi_\nu(\mathbf{k}_j, \mathbf{r})|^2\, w_{\nu j}. \tag{3.36}$$

Because we are dealing with a *non-magnetic* case, a factor "2" is added to account for the spin degeneracy.

In the interstitial region the wave functions are represented in the form

$$\psi_\nu(\mathbf{k},\mathbf{r}) = \frac{1}{\sqrt{\Omega}} \sum_{\mathbf{G}} c^\nu_{\mathbf{G}}(\mathbf{k}) \mathrm{e}^{i(\mathbf{k}+\mathbf{G})\cdot\mathbf{r}}. \tag{3.37}$$

Starting from Eq. (3.36) the electron density in the interstitial region is given by:

$$n(\mathbf{r}) = \frac{2}{\Omega} \sum_{\nu j} w_{\nu j} \sum_{\mathbf{G}\,\mathbf{G}'} c^{\nu\,*}_{\mathbf{G}}(\mathbf{k}_j) c^\nu_{\mathbf{G}'}(\mathbf{k}_j)\, \mathrm{e}^{i(\mathbf{G}'-\mathbf{G})\cdot\mathbf{r}}. \tag{3.38}$$

The electron density in the interstitial region is also expanded into a Fourier series, and the Fourier coefficients of expansion are

$$\begin{aligned} n_{\mathbf{G}''} &= \frac{1}{\Omega}\int_\Omega n(\mathbf{r})\, \mathrm{e}^{-i\mathbf{G}''\cdot\mathbf{r}}\, d^3r \\ &= \frac{2}{\Omega} \sum_{\nu j} w_{\nu j} \sum_{\mathbf{G}\,\mathbf{G}'} c^*_{\mathbf{G}} c_{\mathbf{G}'} \frac{1}{\Omega}\int_\Omega \mathrm{e}^{i(\mathbf{G}'-\mathbf{G}-\mathbf{G}'')\cdot\mathbf{r}}\, d^3r \\ &= \frac{2}{\Omega} \sum_{\nu j} w_{\nu j} \sum_{\mathbf{G}\,\mathbf{G}'} c^*_{\mathbf{G}} c_{\mathbf{G}'}\, \delta_{\mathbf{G}'-\mathbf{G},\mathbf{G}''}. \end{aligned} \tag{3.39}$$

Now consider the $\mathbf{k}$-dependent density (i.e. inner summation in equation above)

$$\begin{aligned} n_{\mathbf{G}''}(\mathbf{k}) &\equiv \sum_{\mathbf{G}\,\mathbf{G}'} \big(c^\nu_{\mathbf{G}}(\mathbf{k})\big)^* c^\nu_{\mathbf{G}'}(\mathbf{k})\, \delta_{\mathbf{G}'-\mathbf{G},\mathbf{G}''} \\ &= \sum_{\mathbf{G}} \big(c^\nu_{\mathbf{G}}(\mathbf{k})\big)^* c^\nu_{\mathbf{G}+\mathbf{G}''}(\mathbf{k}), \end{aligned} \tag{3.40}$$

which is a discrete correlation in momentum space. For each coefficient a sum over $\mathbf{G}$ has to be performed. However, we can calculate it more efficiently by using the FFT. First, we take the Fourier transform of $c^\nu_{\mathbf{G}}(\mathbf{k})$ to real space and square them on a real space mesh, then all bands are summed up, and finally we perform the inverse Fourier transform yielding the results of Eq. (3.40)

In the αth MT sphere the wave function can be written as

$$\psi_\nu(\mathbf{k},\mathbf{r}) = \sum_L \big[\tilde{A}_{L,\nu}(\mathbf{k}) u_\ell(r') + \tilde{B}_{L,\nu}(\mathbf{k}) \dot{u}_\ell(r')\big] Y_L(\hat{\mathbf{r}}'), \tag{3.41}$$

where we have defined the band dependent coefficients $\tilde{A}$ and $\tilde{B}$ as

$$\tilde{A}_{L,\nu}(\mathbf{k}) = \sum_{\mathbf{G}} c^\nu_{\mathbf{G}}(\mathbf{k})\, A_L(\mathbf{k}_{\mathbf{G}}), \qquad \tilde{B}_{L,\nu}(\mathbf{k}) = \sum_{\mathbf{G}} c^\nu_{\mathbf{G}}(\mathbf{k})\, B_L(\mathbf{k}_{\mathbf{G}}). \tag{3.42}$$

Substituting Eq. (3.41) into (3.36) yields the electron density in the muffin-tin sphere as

$$n(\mathbf{r}) = 2\sum_{\nu j} w_{\nu j} \sum_{L} \left[\tilde{A}_L u_\ell + \tilde{B}_L \dot{u}_\ell\right]^* Y_L^* \sum_{L'} \left[\tilde{A}_{L'} u_{\ell'} + \tilde{B}_{L'} \dot{u}_{\ell'}\right] Y_{L'}. \tag{3.43}$$

If we multiply (3.43) with $\int d\hat{\mathbf{r}}'\, Y_{L''}^*$ and use the property that the Gaunt coefficients are real, we have an expansion of the electron density within a MT sphere in terms of spherical harmonics, with the radial electron density functions as

$$\begin{aligned} n_{L''}(r) = \sum_{\nu j} w_{\nu j} \sum_{L\,L'} \big[\, & \tilde{A}_L^* \tilde{A}_{L'}\, u_\ell u_{\ell'} + \tilde{A}_L^* \tilde{B}_{L'}\, u_\ell \dot{u}_{\ell'} \\ & + \tilde{B}_L^* \tilde{A}_{L'}\, \dot{u}_\ell u_{\ell'} + \tilde{B}_L^* \tilde{B}_{L'}\, \dot{u}_\ell \dot{u}_{\ell'} \big]\, \mathcal{G}(L', L, L''). \end{aligned} \tag{3.44}$$

3.5.1 Generating the density for the next iteration

According to the Hohenberg-Kohn theorem, the goal is to minimize the energy functional with respect to the electron density. Within the Kohn-Sham approach this minimization is performed implicitly, by the determination of a self-consistent electron density $n(\mathbf{r})$. As discussed in the Section 2.1.2, given a density n_{in}, the KS equations are constructed and solved, and an output density n_{out} is calculated from the resulting wave functions. This new obtained density will be the input for the next iteration in the self-consistency cycle. However, it may lead to instabilities in the iterative self-consistent process. In order to improve the convergence, some mixing between input and output density is required.

The simplest mixing scheme is straight mixing. That is,

$$n_{in}^{i+1} = (1-\beta) n_{in}^{i} + \beta\, n_{out}^{i}, \tag{3.45}$$

where the superscript refers to the iteration index and β is the mixing parameter. For sufficient small β (~ 0.1) the iteration converges and is very stable.

3.6 Computation of the potential

After we have obtained the total electron density, the next step is to generate the effective potential in Eq. (2.5) due to the charge distribution $\rho(\mathbf{r})$ that relates to

the electron density by

$$\rho(\mathbf{r}) \;=\; -e\, n(\mathbf{r}).$$

We will separate the potential into the Coulomb potential and exchange-correlation potential because calculation of each potential is quite different. In addition, we approximate the starting potential for the first round of iteration by the spherical symmetric atomic potential plus contributions from neighboring atoms [29].

3.6.1 The Coulomb potential: pseudocharge method

The Coulomb potential, which consists the potential due to all electrons called Hartree potential, has to be determined from the charge density via Poisson's equation:

$$\nabla^2 V(\mathbf{r}) = -4\pi\rho(\mathbf{r}). \tag{3.46}$$

It is easier to solve Poisson's equation for an infinite periodic system in Fourier space, such that the solution is simply

$$V(\mathbf{G}) = -\frac{4\pi\rho(\mathbf{G})}{G^2}. \tag{3.47}$$

The $G = 0$ component is arbitrarily set to zero by the condition of charge neutrality. In general, the Fourier expansion of the charge density will be slowly converged because of the large oscillations near the nuclei, whereas the interstitial charge density is fairly smooth. We therefore represent the charge density inside the sphere by a considerably smoother function. Fortunately, Weinert [3] has developed a method for solving Poisson's equation, especially for the charge density represented as in Eq. (2.26).

The pseudocharge method is a very elegant technique to obtain the Coulomb potential in the FLAPW method. The underlying idea is to divide the solution of Poisson's equation into two steps: (1) obtain the potential in the interstitial region and then (2) solve the boundary value problem inside the muffin-tin spheres.

The potential in the interstitial region is dependent on the charge density outside and inside the MT sphere. However, the potential in this region due to a charge distribution within the sphere can be determined completely by its *multipole moments*, without the actual form of the charge density. The same

potential outside the sphere could be obtained from the mutipole expansion of the charge density (including the nucleus) inside the MT sphere. This arbitrariness gives us the freedom to replace the real charge density by a pseudocharge density, i.e.,

$$\rho(\mathbf{r}) \rightarrow \tilde{\rho}(\mathbf{r}) = \rho_I(\mathbf{r})\Theta(\mathbf{r} \in \mathrm{I}) + \sum_{\alpha} \tilde{\rho}_{\alpha}(\mathbf{r})\Theta(\mathbf{r} \in \mathrm{MT}_{\alpha}), \tag{3.48}$$

where $\Theta(\mathbf{r})$ is the unit step function, with the requirement that the pseudocharge density in the spheres have the same multipole moments as the original charge. This pseudocharge density will give the correct interstitial potential, but not the correct potential in the spheres. Because $\tilde{\rho}(\mathbf{r})$ is constructed to have a more rapidly convergent Fourier expansion than the original $\rho(\mathbf{r})$, Poisson's equation can now be solved using Eq. (3.47). Thus

$$V_{\mathrm{I}}(\mathbf{G}) = -\frac{4\pi\tilde{\rho}(\mathbf{G})}{G^2} \ . \tag{3.49}$$

Since the potential in the interstitial region including at the muffin-tin sphere boundary is already known, the potential inside the muffin-tin spheres is just a boundary value problem, which can be solved by means of a standard *Green's function* technique (e.g. [30]):

$$V^{\alpha}_{\mathrm{MT}}(\mathbf{r}) \ = \ \int_{\mathrm{MT}^{\alpha}} \rho_{\alpha}(\mathbf{r}')G(\mathbf{r},\mathbf{r}')\, d^3r' \ - \ \frac{R^2_{\alpha}}{4\pi} \oint_{\mathrm{MT}^{\alpha}} V_{\mathrm{I}}(\mathbf{R}'_{\alpha})\, \frac{\partial G}{\partial n'}\, d\hat{\mathbf{r}}' \ , \tag{3.50}$$

where $G(\mathbf{r},\mathbf{r}')$ is the Green's function for Dirichlet boundary conditions and $\frac{\partial G}{\partial n'}$ is its normal derivative on the sphere boundary. The first integral includes the true charge density and is over the volume while the second integral is over the surface of the muffin-tin sphere. By using the representation of the charge density inside the sphere and calculating the spherical harmonic components of V_{I} on the sphere, we obtain the radial functions of the expansion of Coulomb potential within the sphere:

$$\begin{aligned} V_{\mathrm{MT},\,L}(r) \ &= 4\pi i^{\ell} \sum_{\mathbf{G}} V_{\mathrm{I}}(\mathbf{G}) j_{\ell}(GR) Y^*_L(\hat{\mathbf{G}}) \Big(\frac{r}{R}\Big)^{\ell} \\ &\quad + \frac{4\pi}{2\ell+1} \Bigg[\frac{1}{r^{\ell}+1} \int_0^r \rho_L(r')\, r'^{\ell+2} dr' \ - \ \frac{Z}{\sqrt{4\pi}} \Big[\frac{1}{r} - \frac{1}{R}\Big] \delta_{\ell,0} \\ &\quad - \frac{r^{\ell}}{R^{2\ell+1}} \int_0^R \rho_L(r') r'^{\ell+2} dr' \ + \ r^{\ell} \int_r^R \rho_L(r')\, r'^{1-\ell} dr' \Bigg], \end{aligned} \tag{3.51}$$

where we have dropped the muffin-tin superscript α for clarity.

3.6.2 The exchange-correlation potential

The exchange-correlation potential in our calculations is based on the local density approximation. According to the Hedin-Lundqvist formula [16], the exchange-correlation potential is given by

$$V_{xc}(\mathbf{r}) = -2\left(1 + 0.0368\, r_s\, \ln(1 + \frac{21}{r_s})\right)\left(\frac{3\, n(\mathbf{r})}{\pi}\right)^{1/3}, \tag{3.52}$$

where r_s is defined in Eq. (2.14). In this case, the exchange-correlation potential $V_{xc}(\mathbf{r})$ is a function that depends *locally* and *non-linearly* on the density at a given position $\mathbf{r}$. This means that V_{xc} must be calculated in real space. Moreover, the charge density is represented differently in the interstitial region and the muffin-tin regions. As a result, the potential in each region will be treated independently. Note that the exchange-correlation energy, ε_{xc}, is calculated in the same way in both regions.

Because the components of the interstitial charge density and of the interstitial potential are stored in reciprocal space, the FFT is used to transform the density into real space mesh. Then the exchange-correlation potential is evaluated on the mesh, i.e. grid point by grid point. Finally, the inverse transform is performed yielding the coefficients of Fourier expansion of V_{xc} which hold for the interstitial region.

In the muffin-tin spheres, the charge density is expanded into radial functions and spherical harmonics. The radial functions are stored on a discrete radial mesh; thus the transform to real space affects only the angular part. The charge density will be synthesized from spherical harmonics on a set of angular points $\hat{\mathbf{r}}_i = (\theta_i, \phi_i)$. The exchange-correlation potential is again evaluated on real space mesh. Thereafter, the result $V_{xc}(\mathbf{r})$ is expanded back in terms of spherical harmonics. The r-dependent coefficients of spherical harmonic expansion can be obtained from

$$V_{xc,L}(r) = \int_0^{2\pi}\int_0^{\pi} V_{xc}(r, \theta, \phi)\, Y_L^*(\theta, \phi)\, \sin\theta\, d\theta\, d\phi. \tag{3.53}$$

The angular integration above can be computed exactly via a *Gauss-Legendre quadrature*. The angular points $\hat{\mathbf{r}}_i$, on which the functions $V_{xc}(r, \hat{\mathbf{r}})$ and $Y_L(\hat{\mathbf{r}})$ will be evaluated, are specified by the integration method. In our calculation 98 points on an angular mesh are used, so the quadrature is exact for all Y_L that $\ell \leq 7$.

3.7 The linearization energy parameters

3.7.1 Determination of the optimal energy parameters

In order to minimize the linearization error, the energy parameters should be chosen as close to band energies as possible. However, the band energies $\varepsilon_\nu(\mathbf{k})$ depend on $\mathbf{k}$ whereas the energy parameters E_ℓ are constants, and the radial functions contribute to the eigenfunctions of different band with different energies. Therefore, deviations between $\varepsilon_\nu(\mathbf{k})$ and E_ℓ have to be accepted.

In the first round of calculation, E_ℓ can be set roughly to the middle of those band by using the empirical Wigner-Seitz rule [31]. The rule is that the energies of such bands range between the values of E_ℓ for which $\partial u_\ell(r', E_\ell) \,/\, \partial r'|_{r'=R_\alpha} = 0$ and $u_\ell(R_\alpha, E_\ell) = 0$. Thus one can find the change of sign in value and slope of the radial functions at the sphere boundary and then take the arithmetic mean as the value of E_ℓ.

For the later round of calculations, an optimal choice of E_ℓ can be obtained from the requirement that energy parameters minimize

$$\sum_\nu \int_{BZ} (\varepsilon_\nu(\mathbf{k}) - E_\ell)^2 \, n_{\nu,\ell}(\mathbf{k}) \, d^3k, \tag{3.54}$$

which is the quadratic error weighted with the amount of charge that contributes to the ℓ-character charge in each band, $n_{\nu,\ell}(\mathbf{k})$. A $\mathbf{k}$-dependent ℓ-like charge is given by

$$n_{\nu,\ell}(\mathbf{k}) = \sum_{m=-\ell}^{\ell} |\tilde{A}_{L,\nu}(\mathbf{k})|^2 + |\tilde{B}_{L,\nu}(\mathbf{k})|^2 N_\ell. \tag{3.55}$$

Setting the derivative of (3.54) with respect to E_ℓ equal to zero yields the optimal energy parameters:

$$E_\ell = \frac{\sum_{\nu j} \varepsilon_\nu(\mathbf{k}_j) \, n_{\nu,\ell}(\mathbf{k}_j) \, w_{\nu j}}{\sum_{\nu j} n_{\nu,\ell}(\mathbf{k}_j) \, w_{\nu j}}, \tag{3.56}$$

where the Brillouin zone integrations has been transformed into weight sums over occupied states.

3.7.2 Multiple energy windows

In many cases it is desirable to distinguish three types of electronic states, namely *core, semi-core* and *valence states*. For instance, Fe has core (1s,2s,2p), semi-core (3s,3p) and valence (3d,4s) states. The core states are those whose the electrons are tightly bound to the nucleus and of course contained entirely in the MT sphere. They lie deeply below the Fermi energy, e.g., 1s orbital of Fe which has an energy about -514 Ry. Such an electron in the core state will behave almost exactly as if it were in a free atom, and it does not participate directly in chemical bonding with other atoms. The valence states are the highest occupied states and always have some significant amount of the electron density outside the MT sphere. These valence states are treated by the LAPW method while the core states are treated in an atomic fashion. The semi-core states, however, are high lying core states with an energy of a few Ry less than that for the valence states, e.g., the 3p states of Fe are 4.3 Ry below the Fermi level. The electrons in the semi-core states are not completely confined inside the MT sphere and thus need special attention.

A problem arises in the semi-core states which have the same ℓ-value as the valence states. The linearization energy parameter E_ℓ must be chosen close to the band energy of interest because the LAPW basis is a good one only for eigenvalues near E_ℓ. Accordingly, if we are interested in the semi-core and valence states which have the same ℓ-character simultaneously, we can have only one correct band within a single set of energy parameters. For example, the 3s and 4s states in Fe, if we choose the energy parameter $E_{(\ell=0)}$ close to 4s, the valence (4s) band will be treated correctly while the semi-core (3s) band will be poorly described. On the other hand, if we set $E_{(\ell=0)}$ for accurate results in the semi-core band, we will have poor results in the valence band. So far, the solutions for this problem are either adding another type of basis functions called a *local orbital* (LO) [32] or using a second set of energy parameters in separate energy window referred to as *multiple windows*.

In a multiple window FLAPW calculation a second set of basis functions which have exactly the same form as in Eq. (2.22) but with different energy parameters is used. One is for the valence states, and the other is for the semi-core states. If the overlap between two windows is neglected, this leads to the solution

of two independent eigenvalue problems per self-consistent iteration. We used this method for treatment of the semi-core states (1s orbital for Li) in our calculation.

Chapter 4

Results and Discussion

We have applied the formalism described in the preceding chapters to calculate the total energy of solid lithium (Li). The calculations have been carried out for various crystal structures and various lattice constants, and the results have been used for determining the crystal stability of Li and the phase transformation due to pressure. In this chapter we present the results of the calculated total-energies, some related quantities derived form the total energies and the calculated electronic structures.

4.1 Convergence test of the total energy

Because of the high degree of numerical accuracy required in the total-energy calculations, we must control the numerical parameters to obtain sensible results. Apart from errors due to the local density approximation and neglecting of the lattice vibrations, the numerical errors can be reduced by using more terms in truncations and finer discretizations. In this section we focus on an analysis of the effects of k-point sampling (or k-mesh) and the number of LAPW basis functions to the accuracy of the calculated total-energies. Large size of the basis set and the k-mesh can provide a good result; however, it might also be wasting lots of computational time. Therefore, we find an optimum choice of the k-mesh and the basis set size by considering the total-energy convergence as a function of these parameters. It is very important to perform this convergence test before doing the real calculations.

Initially, we can take a small but sufficient basis set size and calculate the total energy as a function of the size of the k-mesh. An example of the results for

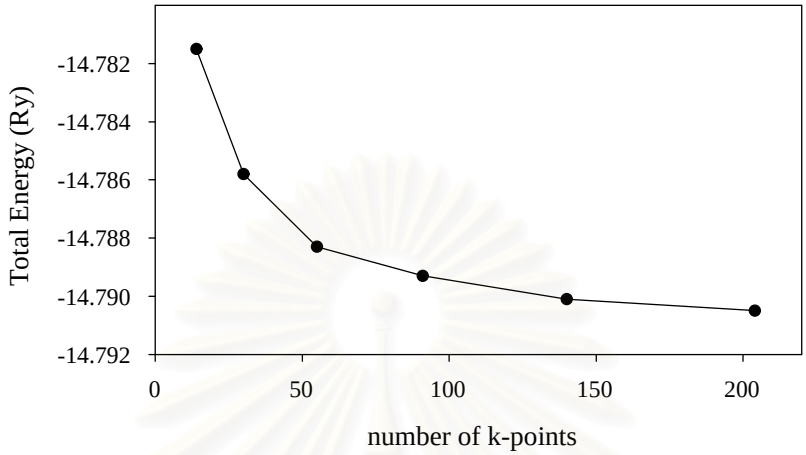

Figure 4.1: An example of total energy as a function of the k-mesh size for the bcc Li with lattice constant $a = 6.63$ a.u.

bcc Li is illustrated in Fig. 4.1, which shows that 204 **k**-points are enough for the total energy that is accurate up to about 0.5 mRy or better. In our calculations, we use 204, 240, 175 and 120 **k**-points in the irreducible Brillouin zone for the bcc, fcc, hcp and sc structures, respectively.

Having determined a good k-mesh, we then change the basis set size. The number of LAPW basis functions are determined by the cutoff parameter G_{max}. However, a better quantity to control the size of basis set here is the dimensionless product $R_{min}G_{max}$ between the smallest muffin-tin radius in the unit cell, R_{min}, and the magnitude of the largest reciprocal vector, G_{max}. This can be understood as follows. If the muffin-tin radius is increased, the interstitial region, in which the wave functions are described by plane waves, is decreased. As a result, less plane waves are needed and G_{max} can be reduced. In the same way, if the muffin-tin radius is decreased, more plane waves are needed and the value of G_{max} increases. The dependence of the total energy of bcc Li on $R_{min}G_{max}$ is shown in Fig. 4.2. It shows that the total energy converges to better than 0.5 mRy for $R_{min}G_{max}$ larger than 9, which corresponds to 79 basis functions. Our calculations has been carried out with an average basis set size of about 70 LAPWs.

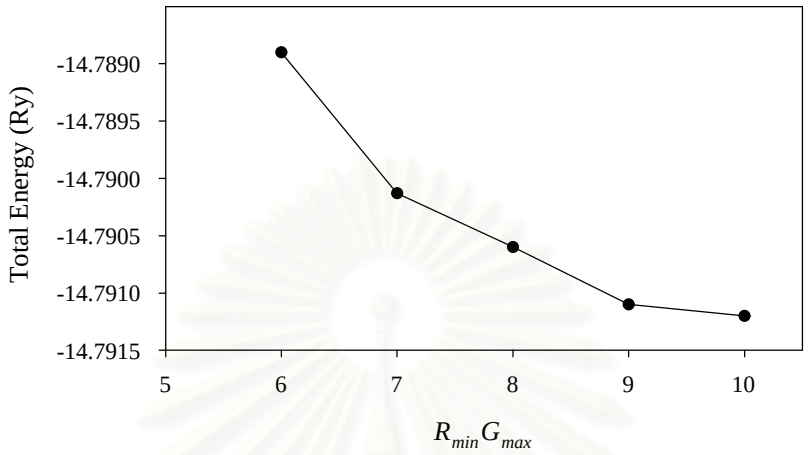

Figure 4.2: A typical total energy as a function of $R_{min}G_{max}$ for the bcc Li with lattice constant $a = 6.63$ a.u. (204 **k** points).

4.2 Static structural properties

The static structural properties such as lattice constant and bulk modulus can be obtained from the calculated total-energies as a function of volume for the observed crystal structure. We have calculated the total energies of the bcc structure of Li for six different atomic volumes around the expected equilibrium volume (or around the volume corresponding to the minimum of total-energy curve). The values of the calculated total energies are then least-squares-fitted to *Murnaghan's equation of states* [33],

$$E_{tot}(V) = \frac{B_0 V}{B_0'}\left[\frac{(V_0/V)^{B_0'}}{B_0' - 1} + 1\right] + const\ , \tag{4.1}$$

where B_0 and B_0' are the bulk modulus and its pressure derivative at the equilibrium volume V_0. This equation of states has been examined and found to be quite accurate for crystals under moderate compression [34]. The minimum total-energy, the equilibrium lattice constant and the bulk modulus are readily deduced from the fitted parameters in the equation of states. The total energies per atom as a function of the atomic volume and the fitted curve are shown in Fig. 4.3.

The least-squares fit to the Murnaghan's equation of states has a root-mean-square (rms) error of about 10^{-5} Ry/atom. By deriving from the fit, the equilib-

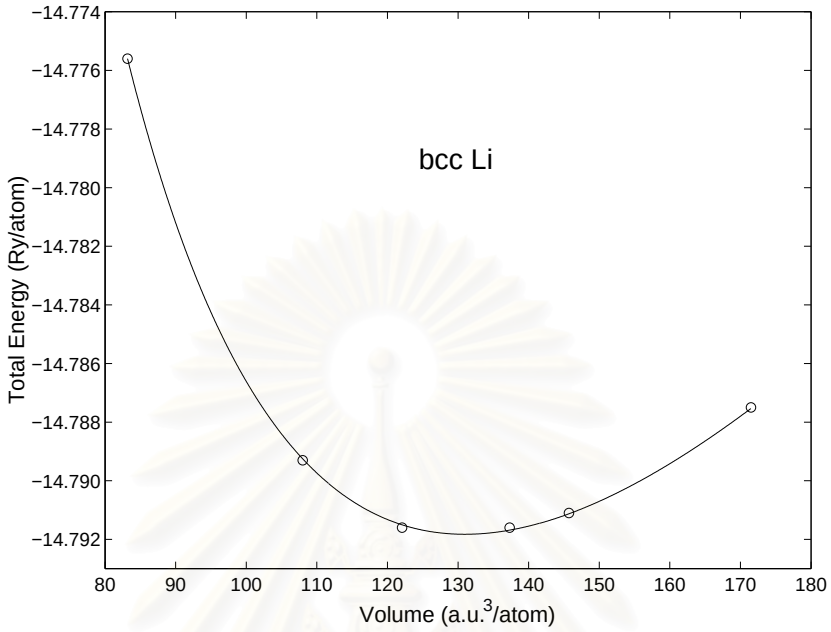

Figure 4.3: The calculated total-energy versus the atomic volume of the bcc Li.

rium atomic volume (V_0) and the bulk modulus (B_0) for bcc Li are founded to be 130.9 a.u.^{3} and 14.7 GPa, respectively, and the calculated value of B_0' is 3.067. The uncertainty of the extracted value of V_0 from the fitting is only 1.5%, and the calculated value of B_0 has a deviation of about 10%. We compare the calculated lattice constants and the bulk moduli with the results from the CASTEP program package [35] (using *ab initio* pseudopotential method) and the experimental results in Table 4.1. In general, the agreement between our calculated results and

Table 4.1: Comparison between the present calculated lattice constant and the bulk modulus with the results from CASTEP calculation and experiment.

	Lattice constant (a.u.)	Bulk modulus (GPa)
Present calculation	6.40	14.7
CASTEP	6.54	13.3
Experiment* [36]	6.50	14.5

*After the effects of finite-temperature and zero-point are removed.

the other results is quite good. The present values for both the equilibrium lattice constant and the bulk modulus agree well with those obtained from CASTEP and from the experiment. The discrepancies between our calculation and the experiment (CASTEP) are about 3% (2%) for the lattice constant, and 1.4% (11%) for the bulk modulus. We note that the experimental results exclude the zero-point and the finite-temperature effects [36], so they can be directly compared to the results of the *ab initio* ground-state calculations with frozen ions.

4.3 Crystal stability

By considering the total energy, the relative stability of different phases can be determined. We calculated the total energies of Li at six different lattice constants for four crystal structures, i.e., sc, bcc, fcc and hcp phases[1]. These data are then least-squares-fitted to the Murnaghan equation of states. The fitted total-energy curves for the four phases of Li are shown in Fig. 4.4. The minimum total-energy per atom ($E_{\min}$), the relative total-energy difference $\triangle E_{\min}$ ($\equiv E_{\min} - E^{\rm fcc}_{\min}$), and the corresponding atomic volume ($V_{\min}$) for each phase of Li are given in Table 4.2. Note that for the hcp structure, the c/a ratio was fixed to the ideal close-packed value of 1.633.

Table 4.2: Shows the volumes at the minimum energies ($V_{\min}$), the minimum energies ($E_{\min}$) and $\triangle E_{\min}$ for the sc, bcc, fcc and hcp structures of Li.

	sc	bcc	fcc	hcp
$V_{\min}$ (a.u.^{3})	131.9825	130.5001	130.0037	130.9999
$E_{\min}$ (Ry)	-14.7830	-14.7918	-14.7920	-14.7919
$\triangle E_{\min}$ (mRy)	11.7	0.2	0	0.1

From these calculations of the total energies of the four phases, we find that the differences of the minimum energies of the fcc-bcc and the fcc-hcp are quite

[1]Most crystal structures for metals are bcc, fcc and hcp.

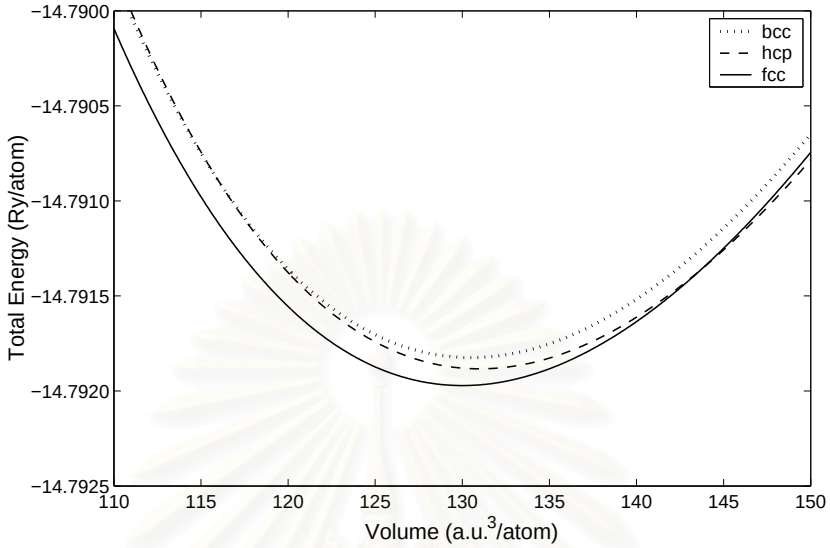

Figure 4.4: Total-energy curves of the three phases of Li as a function of the atomic volume. The dotted curve is for the bcc phase, dash curve for the hcp phase, and solid curve for the fcc phase.

small, and less than the size of error in the total energy. Therefore, the comparison of the total energies among these phases to predict the preferred crystal structure cannot be reliable. However, the total energies of the fcc phase are less than the total energies of other phases at all considered volumes. This make us to believe that the total-energy curve of the fcc phase should be lowest in energy, and thus the fcc phase is possibly the most stable phase among the four phases of Li. This is in agreement with the previous calculations [37, 38, 39, 40, 41] which reported that the fcc is the stable phase. In addition, the difference in energy between the fcc and hcp phases of ours is considerably large when compare to the similarity of the fcc and hcp structures.

Lithium may undergo a structural phase transformation if pressure is applied. Prior studies suggested that the bcc structure is stable at high pressure. However, there is no fcc-bcc transition in our results. We find that the total energies of the fcc structure become relatively lower than that of the bcc structure for all volumes we considered. That is, the fcc phase holds the stability for pressures up to about 10 GPa. This is consistent with results of Meyer-ter-Vehn [42] that Li transforms from the fcc structure to the bcc structure at the pressure of 400 GPa, which is much higher pressure than that considered in this work.

4.4 Electronic structure and charge density

In this section, we present the results of the electronic structure calculations for the fcc phase of Li at the equilibrium volume and at a compressed volume. The calculated band structures and the density of states are shown in Fig. 4.5, and they were obtained by solving self-consistently the Kohn-Sham equations. Although the one-electron eigenvalues obtained from density functional theory have no rigorous physical interpretations, the band structures near the Fermi level are believed to correlate well with electronic excitation energies in metals. Our results are similar to that from other *ab initio* calculations [37, 39].

The band structures shown in Fig. 4.5 correspond to the band structures of the fcc Li at zero pressure (dotted line) and also at the pressure of 10 GPa (solid line). The lowest band is 2s band, and the next three bands are 2p bands. The Fermi level is determined by calculating the integrated density of states (or number of states[2] as a function of energy) [28]. The occupied part of the band structures is parabolic with the minimum energy at the Γ point. This is like the free-electron case. Under pressures up to 10 GPa, the shape of the band structure remains unchanged. However, all of the bands are broaden by pressures, and the p band is broaden more rapidly than the s band. The 1s band is narrow and lies deeply below the valence-band. (It is not plotted in the Figure.) At zero pressure, it is 0.003 Ry wide, and the difference between the lowest of 2s band and the top of 1s band is 3 Ry. The 1s band, however, moves closer to the 2s band as the pressure increases. The separation between 1s and 2s band decreases to 1.24 Ry at 10 GPa. In addition, pressures lead to raising up in Fermi level. (In the Figure, the energies of both band structures are shifted to have the Fermi levels at zero.) The Fermi energy becomes 0.086 Ry higher than that for the zero pressure.

In order to visualize the chemical bonding directly, we present the result of the valence charge density for the fcc Li at zero pressure in Fig. 4.6. The contour plot is shown for a cross-section in the (001) plane, and we have plotted the (valence) charge density along the line between two atoms in the [100] direction. Notice that most of the charge density is spherical symmetric around the regions near the atomic sites and some small charge density is flat in the interstitial region.

[2]The number of occupied states is equal to the number of electrons.

This characteristic of the charge distribution indicates the metallic bonding. The plot in Fig. 4.6(b) shows the similar results of the charge density under pressure of 10 GPa, compared to the zero-pressure density.

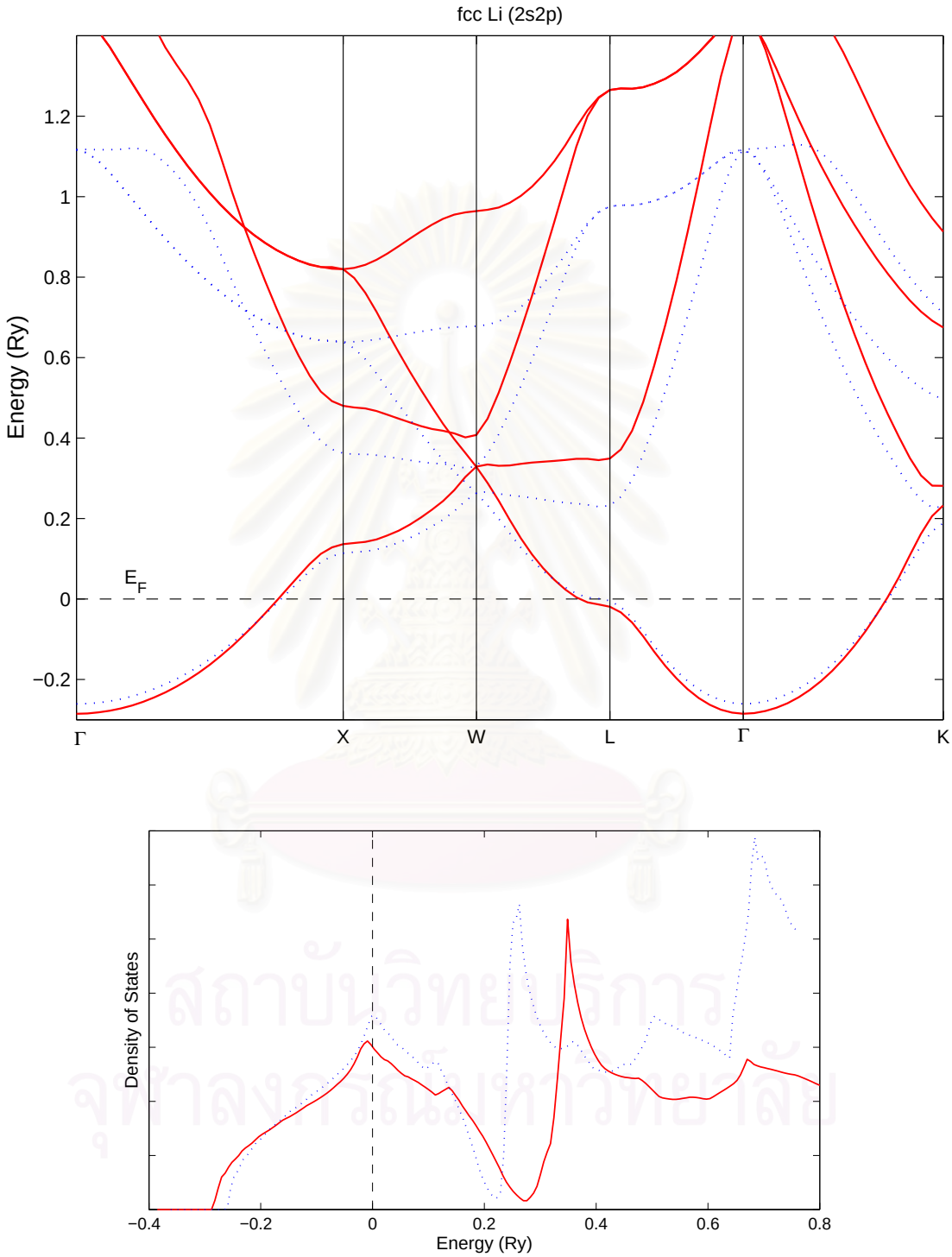

Figure 4.5: The band structures and the density of states of the fcc Li. The band structures are plotted along the symmetry lines. The energies are shifted so that the Fermi level is zero. The dotted line is the result at the equilibrium volume (lattice constant = 8.041 a.u.) while the solid line is at 0.69 times the equilibrium volume.

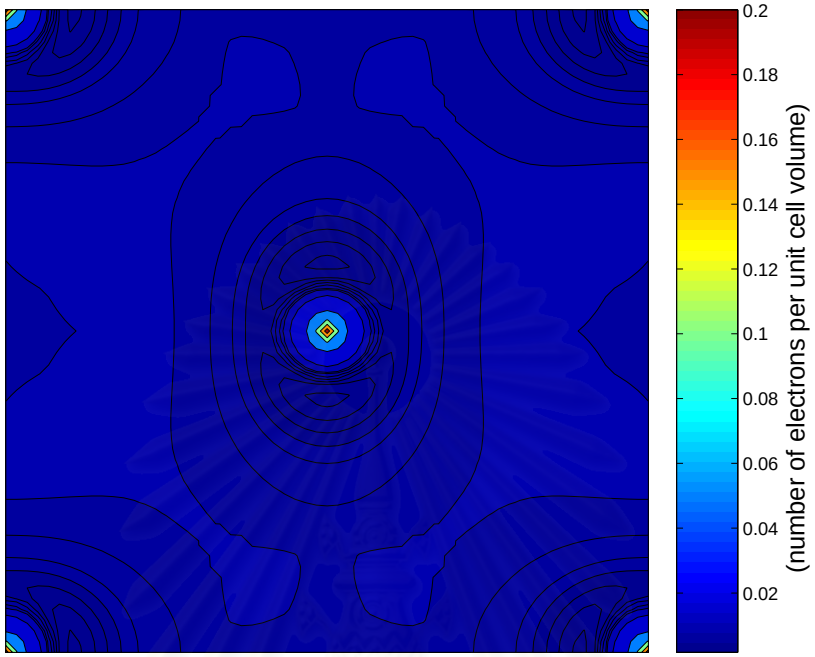

(a)

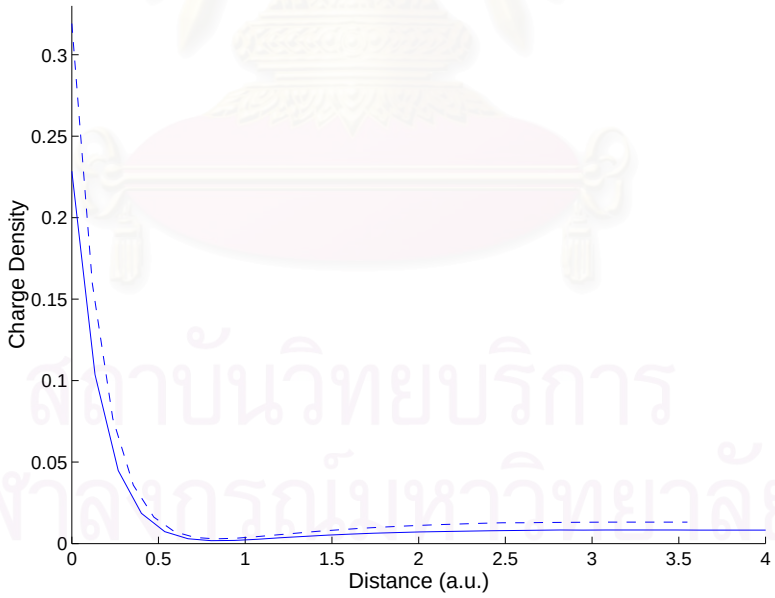

(b)

Figure 4.6: (a) The Contour plot of the valence charge density in the (001) plane of the fcc phase of Li at the zero pressure. (b) The Plot of the charge density in the [100] direction. The solid line is for zero pressure whereas the dash line is for 10 GPa.

Chapter 5

Conclusions

In summary, we have developed and implemented an accurate total-energy method based on the local-density-functional theory and the full-potential linearized augmented-plane-wave method. In order to check the accuracy of our algorithm, we have performed calculations of the total energy to determine the structural properties of solid lithium. Our calculated results are generally in agreement with previous calculations and experiments.

The total energies calculated here do not include thermal effects, i.e. zero-point energy, and exchange-correlation effects are treated under the local density approximation. All numerical approximation are controlled in effort to achieve the high accurate results. We have demonstrated the convergence of the total energy with respect to the computational parameters by using different basis set sizes and different k-mesh sizes. The test done with a larger number of basis functions and k-point sampling leads us to believe that the overall accuracy of the total energies are better than 0.5 mRy.

In our application to Li, the results of the equilibrium lattice constant and the bulk modulus agree very well with the results from CASTEP calculation and experiments. Moreover, we predict that at $T = 0$ K the fcc structure is more stable than the sc, bcc and hcp structures. This is consistent with the previous calculations. However, we are suspicious about the large energy difference between the fcc and hcp structures, compared to the similarity of both structures. This may be due to use of non-optimal value of c/a ratio. Although we can conclude the zero-pressure phase stability, we cannot resolve the pressure-induced phase transition. Our calculation holds for pressures up to 10 GPa while the phase transition to the bcc structure is predicted to be at higher pressures.

Although the DFT-FLAPW approach can be used to provide a reliable structural information, our *ab initio* simulations cannot be used to perform structural optimization directly. We must select a certain set of crystal structures. Some of the structures, however, will have extra parameters, e.g. c/a ratios, which must be optimized. Therefore, we can only determine statically which structure is stable among those structures included in the set. In that way one can never be sure to find the *true* ground state structure.

Not only the structural properties, we can determine also the electronic properties. The results of the band structure and the charge density are consistent with other data. These results show that Li becomes free-electron like, and it changes slightly under the moderate pressure.

In the future, we intend to continue to refine and improve the efficiency and reliability of our algorithm as time and opportunity permit. Furthermore, the DFT-FLAPW calculations is universal applicable, many materials problems can be studied through this method. We, therefore, aim to extend our code to many applications, for example, to study the properties of other elements as well as surfaces or molecules.

References

[1] M.T. Yin and Marvin L. Cohen. Theory of static structural properties, crystal stability, and phase transformations: Application to Si and Ge. *Phys. Rev. B* **26** (1982): 5668.

[2] E. Wimmer, H. Krakauer, M. Weinert, and A.J. Freeman. Full-potential self-consistent linearized-augmented-plane-wave method for calculating the electronic structure of molecules and surfaces: O_2 molecule. *Phys. Rev. B* **24** (1981): 864.

[3] M. Weinert. Solution of Poisson's equation: Beyond Ewald-type methods. *J. Math. Phys.* **22** (1981): 2433.

[4] M. Weinert, E. Wimmer, and A.J. Freeman. Total-energy all-electron density functional method for bulk solids and surfaces. *Phys. Rev. B* **26** (1982): 4571.

[5] P. Blaha, K. Schwarz, P. Sorantin, and S.B. Trickey. Full-potential linearized augmented plane wave programs for crystalline solids. *Comput. Phys. Commun.* **59** (1990): 399.

[6] P. Blaha and K. Schwarz. *Int. J. Quantum Chem.* **23** (1983): 1535.

[7] H.J.F. Jansen and A.J. Freeman. Total-energy full-potential linearized augmented-plane-wave method fo bulk solids: Electronic and structural properties of tungsten. *Phys. Rev. B* **30** (1984): 561.

[8] P. Blaha, K. Schwarz, and P. Herzig. First-principles calculation of the electric field gradient of Li_3N. *Phys. Rev. Lett.* **54** (1985): 1192.

[9] S.H. Wei, H. Krakauer, and M. Weinert. Linearized augmented-plane-wave calculation of the electronic structure and total energy of tungsten. *Phys. Rev. B* **32** (1985): 7792.

[10] L.F. Mattheiss and D.R. Hamann. Linear augmented-plane-wave calculation of the structural properties of bulk Cr, Mo, and W. *Phys. Rev. B* **33** (1986): 823.

[11] A.W. Overhauser. Crystal structure of lithium at 4.2 K. *Phys. Rev. Lett.* **53** (1984): 64.

[12] J.B. Neaton and N.W. Ashcroft. Pairing in dense lithium. *Nature* **400** (1999): 141.

[13] M. Hanfland, K. Syassen, N.E. Christensen, and D.L. Novikov. New high-pressure phases of lithium. *Nature* **408** (2000): 174.

[14] P. Hohenberg and W. Kohn. Inhomogeneous electron gas. *Phys. Rev.* **136** (1964): B864.

[15] W. Kohn and L. Sham. Self-consistent equations including exchange and correlation effects. *Phys. Rev.* **140** (1965): A1133.

[16] L. Hedin and B.L. Lundqvist. Explicit local exchange-correlation potentials. *J. Phys. C* **4** (1971): 2064.

[17] T.L. Loucks. *Augmented Plane Wave method: A Guide to Performing Electronic Structure Calculations.* Benjamin, New York, 1967.

[18] J.C. Slater. Wave functions in a periodic potential. *Phys. Rev.* **51** (1937): 846.

[19] O.K. Andersen. Linear methods in band theory. *Phys. Rev. B* **12** (1975): 3060.

[20] D.D. Koelling and G.O. Arbman. Use of energy derivative of the radial solution in an augmented plane wave method: application to copper. *J. Phys. F* **5** (1975): 2041.

[21] D.J. Singh. *Planewaves, Pseudopotential and the LAPW Method.* Kluwer Academic Publishers, Boston, 1994.

[22] E. Sjöstedt, L. Nordström, and D.J. Singh. An alternative way of linearizing the augmented plave wave method. *Phys. Rev. B* **114** (2000): 15.

[23] G.K.H. Madsen, P. Blaha, K. Schwarz, and E. Sjöstedt. Efficient linearization of the augmented plave wave method. *Phys. Rev. B* **64** (2001): 195134.

[24] Franz J. Vesely. *Computational Physics: An Introduction*, 2nd edition. Kluwer Academic, New York, 2001.

[25] George B. Arfken and Hans J. Weber. *Mathematical Method for Physicists*, 5th edition. Harcourt/Academic Press, San Diego, 2001. Section 12.8.

[26] George B. Arfken and Hans J. Weber. *Mathematical Method for Physicists*, 5th edition. Harcourt/Academic Press, San Diego, 2001. Section 12.9.

[27] M.E. Rose. *Elementary Theory of Angular Momentum.* Wiley, New York, 1957. pages 61-62.

[28] P.E. Blöchl. Improved tetrahedron method for Brilliouin-zone integrations. *Phys. Rev. B* **49** (1994): 16223.

[29] L.F. Mattheiss. Energy Bands for Solid Argon. *Phys. Rev.* **133** (1964): 184.

[30] J.D. Jackson. *Classical Electrodynamics*, 2nd edition. Wiley, New York, 1975. Section 3.10.

[31] O.K. Andersen. Simple approach to the band-structure problem. *Solid State Communications* **13** (1973): 133.

[32] D.J. Singh. Ground-state properties of lanthanum: Treatment of extended-core states. *Phys. Rev. B* **43** (1991): 6388.

[33] F.D. Murnaghan. The compressibility of media under extreme pressurre. *Proc. Nat. Acad. Sci U.S.A.* **30** (1944): 244.

[34] O.L. Anderson. The use of ultrasonic measurements under modest pressure to estimate compression at high pressure. *J. Phys. Chem. Solids* **27** (1966): 547.

[35] M.D. Segall, P.L.D. Lindan, M.J. Probert, C.J. Pickard, P.J. Hasnip, S.J. Clark, and M.C. Payne. First-principles simulation: ideas, illustrations and the castep code. *J. Phys.: Cond. Matt.* **14** (2002): 2717.

[36] R. Gaudoin and W.M.C. Foulkes. *Ab initio* calculations of bulk moduli and comparison with experiment. *Phys. Rev. B* **66** (2002): 052104.

[37] J.C. Boettger and S.B. Trickey. Equation of state and properties of lithium. *Phys. Rev. B* **32** (1985): 3391.

[38] J.C. Boettger and R.C. Albers. Structural phase stability in lithium to ultra-high pressures. *Phys. Rev. B* **39** (1989): 3010.

[39] M. Sigalas, N.C. Bacalis, D.A. Papaconstantopoulos, M.J. Mehl, and A.C. Switendick. Total-energy calculations of solid H, Li, Na, K, Rb, and Cs. *Phys. Rev. B* **42** (1990): 11637.

[40] Amy Y. Liu, Andrew A. Quong, J.K. Freericks, E.J. Nicol, and Emily C. Jones. Structural phase stability and electron-phonon coupling in lithium. *Phys. Rev. B* **59** (1999): 4028.

[41] K. Doll, N.M. Harrison, and V.R. Saunders. A density functional study of lithium bulk and surfaces. *J. Phys.: Condens. Matter* **11** (1999): 5007.

[42] J. Meyer-ter-Vehn and W. Zittel. Electronic structure of matter at high compression. *Phys. Rev. B* **37** (1988): 8674.

APPENDICES

Appendix A

Flow chart

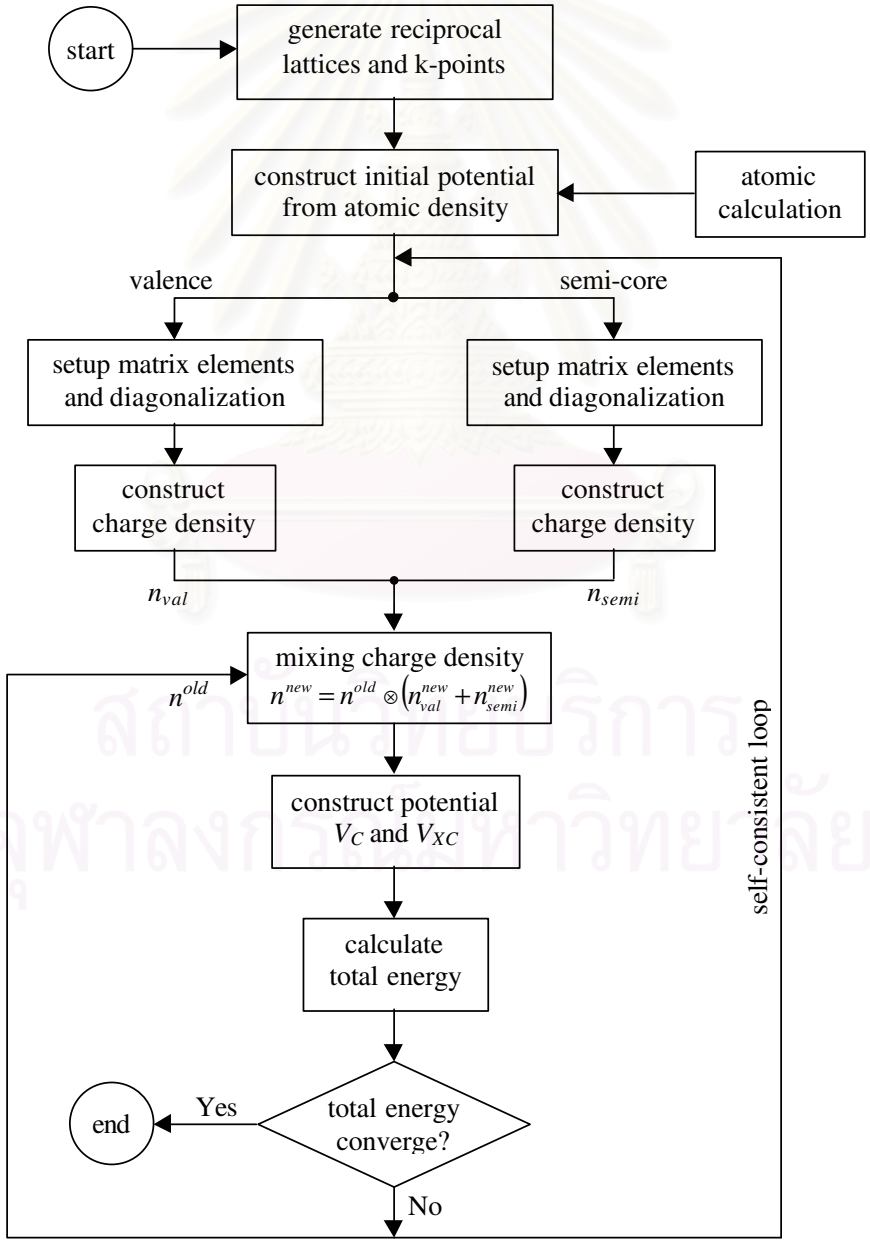

Appendix B

Numerov method

Numerov's method is an efficient algorithm for numerically integrating a second-order differential equation of the form

$$\frac{d^2y}{dx^2} = F(x)y + G(x), \tag{B.1}$$

where $F(x)$ and $G(x)$ are functions with values either known or calculable. This equation appears in many areas of physics (e.g. 1D Schrödinger equation and motion of an undamped forced harmonic oscillator). The important property of this equation is that it contains no first derivative term and the RHS is linear in the dependant variable.

In order to obtain a finite-difference form of Eq. (B.1), the continuous space x is replaced by a uniform grid point, x_n, with a separation of Δx. Now, consider a Taylor series expansion of $y(x)$ about a point x_n,

$$y_{n\pm1} \;=\; y_n \pm \Delta x\, y'_n + \frac{(\Delta x)^2}{2}\, y''_n \pm \frac{(\Delta x)^3}{6}\, y'''_n + \frac{(\Delta x)^4}{24}\, y^{(4)}_n \pm \ldots \tag{B.2}$$

where $y_n \equiv y(x_n)$ is the value of y at x_n and $y_{n\pm1} = y(x_n \pm \Delta x)$. Adding the Taylor formulae for y_{n+1} and y_{n-1} up to fourth order, one finds

$$y_{n+1} + y_{n-1} = 2y_n + (\Delta x)^2 y''_n + \frac{(\Delta x)^4}{12}\, y^{(4)}_n + O[(\Delta x)^6]. \tag{B.3}$$

Differentiating Eq. (B.3) twice and neglecting the last term,

$$y''_{n+1} + y''_{n-1} = 2y''_n + (\Delta x)^2 y^{(4)}_n, \tag{B.4}$$

and substituting the fourth derivative $y^{(4)}_n$ from this into Eq. (B.3) yields

$$y_{n+1} + y_{n-1} = 2y_n + (\Delta x)^2 y''_n + \frac{(\Delta x)^4}{12}\,[y''_{n+1} + y''_{n-1} - 2y''_n] + O[(\Delta x)^6]. \tag{B.5}$$

Inserting for $y''_n, y''_{n\pm1}$ from the original equation Eq. (B.1), one arrives at Numerov's formula:

$$y_{n+1} = \left[\left(2 + \frac{10(\Delta x)^2}{12}F_n\right)y_n - \left(2 + \frac{(\Delta x)^2}{12}F_{n-1}\right)y_{n-1} + \frac{(\Delta x)^2}{12}(G_{n+1} + 10G_n + G_{n-1})\right] \Big/ \left(1 - \frac{(\Delta x)^2}{12}F_{n+1}\right). \tag{B.6}$$

Note that this formula has an error of $O[(\Delta x)^6]$.

To start Numerov's algorithm, values for y_0 and y_1 are needed. Then y_2, y_3, ... can be generated from Eq. (B.6).

Vitae

Mr. Apirath Phusittrakool was born on 14 Febuary 1979 in Bangkok, Thailand. He received his Bachelor degree of Science in Physics from Chulalongkorn University in 1998.

Conference Presentations:

2004 A. Phusittrakool and U. Pinsook. Total-energy full-potential linearized augmented-plane-wave for bulk solids: structural properties of lithium. *12th Annual Academic Conference*, Faculty of Science, Chulalongkorn University (18-19 March 2004): PH 4

2003 A. Phusittrakool and U. Pinsook. Self-consistent band-structure calculation of metallic hydrogen by the FLAPW method. *29th Congress on Science and Technology of Thailand*, Khon Kaen University (20-22 October 2003): SD-48O